Chapter 5

Validation of analytical downburst wind load calculation methods

5.1 Introduction

The wind-excited response of structures due to transient downburst events has been studied by many researchers since Choi and Tanurdjaja (2002) highlighted the possible underestimation of response when the classical approach of the gust response factor is applied to the downburst excited response of SDOF systems. Consequently, different aspects of the wind load and response modeling have been studied by solving the equation of motion in the time domain (Brusco et al., 2019; Brusco and Solari, 2021; Chay and Albermani, 2005; Chen and Letchford, 2004a,b).

Holmes et al. (2005) proposed the general idea of a response factor whose interpretation is analogous to the response spectrum technique in earthquake engineering. This idea was further developed and extended for multiple degrees of freedom systems resulting in the first thunderstorm response spectrums using multiple wind speed records of downbursts (Solari, 2016; Solari and De Gaetano, 2018; Solari et al., 2015b).

Chen (2008) created a framework for calculating the alongwind response in the time-frequency domain through evolutionary power spectral density. He simplified the framework assuming a uniformly modulated fluctuating component for application in the alongwind response calculation of a tall building and the simplification allowed for the definition of the root mean square (RMS) of the response fluctuation from frequency domain analysis. Consequently, the assumption of uniformly modulated fluctuating wind resulted in other approaches for the calculation of the dynamic response of structures due to transient winds in the frequency domain (Kwon and Kareem, 2009, 2013, 2019; Roncallo and Solari, 2020; Roncallo et al., 2022).

Besides, new approaches for the response estimation considering the non-linearity of structural properties and the coupling of the equation of motion due to motion-dependent aeroelastic forces were studied through novel approaches (Le and Caracoglia, 2015a,b, 2017).

In this chapter, the two approaches are thoroughly discussed, compared, and validated highlighting their sources of uncertainties. The comparison was done using the 93 thunderstorm wind speed records that were previously used to drive the TRS method, and comparing the resulting gust response factor with the one obtained using the G-GFF method, for a wide range of structures on a similar basis. In addition, both methods were validated using the full-scale wind-and-structural-response data registered during two case studies of downburst events. In most structural response monitoring studies, only the fluctuating part of the response is retrieved using acceleration records because of the difficulty of monitoring displacement. However, in this study, both the quasi-static and resonant parts of the structural response were retrieved using strain measurements. This was pivotal for the validation of the two methods. In Section 5.2, the derivation of the thunderstorm response spectrum technique is briefly revised, a proposal for some modification is given and the method is validated using full-scale monitoring data of the two case studies of downburst. In Section 5.3, the generalized gust front factor is derived and validated using full-scale monitoring data of the two case studies of downburst events. In Section 5.4, a detailed comparison between the two methods is made highlighting their sources of uncertainty. Finally, conclusions are made and prospects for future research are recommended in Section 5.5.

5.2 Thunderstorm response spectrum technique (TRS) method

5.2.1 Background

The response spectrum technique is widely applied in earthquake engineering for the design of structures against seismic loads. Response spectrum is the peak response of SDOF structures, with various damping and natural frequency, under a registered ground acceleration (Chopra, 2014). It is usually plotted as a function of the natural frequency for different assumptions of damping, resulting in the response spectrum curves. The primary inputs of the earthquake response spectrum are the collected ground acceleration time histories at different locations around the world during past seismic events. The resulting response spectrum curves are dependent on the input ground acceleration time history's intensity; lower-intensity ground accelerations will result in a low response spectrum and high-intensity ground accelerations will result in a high response spectrum. In order to obtain a response spectrum that is not dependent on the ground acceleration intensity, the ground acceleration time histories are usually

normalized with respect to their respective peak values. The design response spectrum is obtained by calculating the response spectrum using numerous inputs of normalized ground accelerations and applying probabilistic approaches.

Thunderstorm outflow winds are random transient events. Looking at this property, Solari et. al. proposed the thunderstorm response spectrum (TRS) method, extending the widely used response spectrum technique in earthquake engineering to the field of wind engineering (Solari, 2016; Solari et al., 2015a; Solari and De Gaetano, 2018). The primary inputs for the thunderstorm response spectrum were the 93 wind speed time histories recorded during thunderstorm outflows by a network of closely spaced anemometers.

The derivation of the thunderstorm response spectrum is presented in Solari et al. (2015a), Solari (2016), and Solari and De Gaetano (2018) for slender structures that can be schematized as cantilevers considering the first mode of vibration only. Since the underlying assumptions of this method will be compared with the G-GFF method in Section 5.4, its derivation is briefly explained in this Section to lay out a foundation for subsequent sections.

Starting from the definition of the wind field model, the wind speed time history, $u(z,t)$, is modeled as a summation of a time-varying mean component, $\bar{u}(z,t)$, and fluctuating component, $u'(z,t)$.

$$u(z,t) = \bar{u}(z,t) + u'(z,t) \tag{5.1}$$

The fluctuating component of the wind speed, $u'(z,t)$, is defined as:

$$u'(z,t) = \sigma_u(z,t)\tilde{u}'(z,t) \tag{5.2}$$

where $\sigma_u(z,t)$ is the time-varying standard deviation of $u'(z,t)$; and $\tilde{u}'(z,t)$ is a normalized stationary fluctuating component.

Defining the time-varying turbulence intensity as $I_u(z,t) = \sigma_u(z,t)/\bar{u}(z,t)$, Eq. 5.1 can be written as:

$$u(z,t) = \bar{u}(z,t)\left[1 + I_u(z,t)\tilde{u}'(z,t)\right] \tag{5.3}$$

The time-varying mean wind speed is defined as:

$$\bar{u}(z,t) = \bar{u}_{max}(h)\alpha(z)\gamma(t) \tag{5.4}$$

where $\bar{u}_{max}$ is the maximum value of the time-varying mean wind speed registered at the anemometric height; h is the height of the anemometer; α is a non-dimensional function of height that defines the shape of the vertical profile of the mean wind speed; γ is a non-dimensional time function with a maximum value of 1.

The time-varying turbulence intensity is defined as:

$$I_u(z,t) = \bar{I}_u(h)\beta(z)\mu(t) \tag{5.5}$$

where $\bar{I}_u$ is the average value of I_u; β is a non-dimensional function of height that defines the shape of the vertical profile of I_u; μ is a non-dimensional function of time that expresses the time variation of I_u.

The normalized fluctuating component, $\tilde{u}'(z,t)$, is considered to have similar properties as the fluctuating component of wind speed in atmospheric boundary layer (ABL) winds. Thus, models of ABL wind's power spectral density and coherence can be used to generate partially correlated fluctuations at various heights. However, instead of generating partially correlated wind fields on various points of the structure using Monte Carlo simulation, a method that replaces the partially correlated wind field with a space invariant perfectly correlated wind field was used. This method is developed by (Solari, 1988) and is known as the equivalent response spectrum technique (EWST). It was developed with the aim that the 1^{st} mode response of the structure due to the partially correlated wind field is equivalent to the 1^{st} mode response of the structure due to the perfectly correlated wind field. Since the coherence of the wind field is dependent on the size of the structure and other parameters such as the wind speed, the equivalent fluctuation is dependent on a size parameter, δ. Thus, EWST was used to replace the height-varying normalized fluctuation, $\tilde{u}'(z,t)$, with an equivalent height invariant normalized fluctuation, $\tilde{u}'_{eq}(t,\delta)$. A more detailed explanation of the EWST application is presented in Chapter 4.

Accordingly, Eq. 5.3 is redefined as:

$$u_{eq}(z,t) = \bar{u}(z,t)\left[1 + I_u(z,t)\tilde{u}'_{eq}(t,\delta)\right] \tag{5.6}$$

Substituting Eq. 5.4 and Eq.5.5 in Eq. 5.6 and assuming $\beta(z) = 1$

$$u_{eq}(z,t,\delta) = \bar{u}_{max}(h)\alpha(z)\gamma(t)\left[1 + \bar{I}_u(h)\mu(t)\tilde{u}'_{eq}(t,\delta)\right] \tag{5.7}$$

Noting that all the parameters except $\alpha(z)$ are height invariant and depend only on the wind speed time history recorded at the anemometric height, h, and the size factor, δ, Eq. 5.7 is written as:

$$u_{eq}(z,t,\delta) = u_{eq}(h,t,\delta)\alpha(z) \tag{5.8}$$

Assuming strip and quasi-steady theory, the maximum aerodynamic force due to the slowly varying mean wind speed is given by:

$$\bar{f}(z) = \frac{1}{2}\rho B(z) C_d(z)[\bar{u}_{max}(h)\alpha(z)]^2 \tag{5.9}$$

where ρ is the air density; B is the width of the structure perpendicular to the alongwind direction; and C_d is the drag coefficient.

The maximum static deflection due to the slowly varying mean wind speed is:

$$\bar{x}_{st} = \frac{1}{m_1\omega_1^2}\int_0^H \bar{f}(z)\psi_1(z)dz \tag{5.10}$$

where m_1 is the generalized first mode mass; ω_1 is the fundamental circular frequency; and ψ_1 is the first mode shape.

Substituting Eq. 5.9 in Eq. 5.10

$$\bar{x}_{st} = \frac{1}{m_1\omega_1^2}\frac{1}{2}\rho\bar{u}_{max}^2(h)\int_0^H B(z)C_d(z)\alpha^2(z)\psi_1(z)dz \tag{5.11}$$

On the other hand, the total aerodynamic force due to the equivalent wind speed, $u_{eq}(z,t,\delta)$, is:

$$f(z,t) = \frac{1}{2}\rho B(z)C_d(z)[u_{eq}(z,t,\delta)]^2 \tag{5.12}$$

Substituting Eq. 5.8 in Eq. 5.12

$$f(z,t) = \frac{1}{2}\rho B(z)C_d(z)u_{eq}^2(h,t,\delta)\alpha^2(z) \tag{5.13}$$

The first mode generalized force is:

$$f_1(t) = \int_0^H f(z,t)\psi_1(z)dz \tag{5.14}$$

Substituting Eq.5.13 in Eq. 5.14

$$f_1(t) = \frac{1}{2}u_{eq}^2(h,t,\delta)\int_0^H B(z)C_D(z)\alpha^2(z)\psi_1(z)dz \tag{5.15}$$

The equation of motion considering only the first mode of vibration is:

$$\ddot{p}_1(t) + 2\xi_1\omega_1\dot{p}_1(t) + \omega_1^2 p_1(t) = \frac{1}{m_1} f_1(t) \tag{5.16}$$

where p_1 is the principal coordinate of the first mode deflection; and ξ_1 is the first mode damping ratio.

Since it is intended to obtain a scaling factor that multiplies the mean static response to get the peak dynamic response, a new parameter $d_{eq}(t)$ was defined as $d_{eq}(t) = p_1(t)/\bar{x}_{st}$. Accordingly $p_1(t)$ becomes

$$p_1(t) = d_{eq}(t)\bar{x}_{st} \tag{5.17}$$

Substituting Eq. 5.17 in Eq. 5.16

$$\ddot{d}_{eq}(t) + 2\xi_1\omega_1\dot{d}_{eq}(t) + \omega_1^2 d_{eq}(t) = \frac{1}{m_1}\frac{f_1(t)}{\bar{x}_{st}} \tag{5.18}$$

Substituting Eq. 5.11 in Eq. 5.18

$$\ddot{d}_{eq}(t) + 2\xi_1\omega_1\dot{d}_{eq}(t) + \omega_1^2 d_{eq}(t) = \left[\frac{u_{eq}^2(h,t,\delta)}{\bar{u}_{max}(h)}\right]^2 \omega_1^2 \tag{5.19}$$

It should be noted that the right side of Eq. 5.19 is dependent only on the wind speed time history recorded at the anemometric height. Thus, solving Eq. 5.19 for a structure with damping ratio, ξ_1, fundamental circular frequency, ω_1, and size factor, δ, for multiple inputs of wind speed time history and extracting the ensemble of $max[d_{eq}]$ gives a single point in the response spectrum. Repeating the procedure for various values of ξ, ω_1, and δ, the thunderstorm response spectrum curves were obtained. The response spectrum calculated following the procedure explained above is termed 'the equivalent "mean" thunderstorm response spectrum', $S^{-}_{d,eq}$, in Solari and De Gaetano (2018). This factor is a scaling factor that multiplies the mean static thunderstorm wind load to get the peak dynamic load.

It can be demonstrated that a response spectrum that multiplies the peak static force to get the peak dynamic response can be derived with a similar procedure assuming that the vertical profile of the peak wind speed is the same as the vertical profile of the mean wind speed. Such response spectrum is termed 'the equivalent thunderstorm response spectrum', $S_{d,eq}$, in Solari and De Gaetano (2018). This factor is a scaling factor that multiplies the peak static thunderstorm wind load/response to get the peak dynamic load/response.

Fig. 5.1 shows the mean value of $S_{d,eq}$ obtained using the 93 wind speed time histories and presented in Solari and De Gaetano (2018), and Fig. 5.2 shows its covariance. Fig. 5.3 shows the mean value of $S^{-}_{d,eq}$ obtained using the 93 wind speed time histories and presented in Solari and De Gaetano (2018), and Fig. 5.4 shows its covariance.

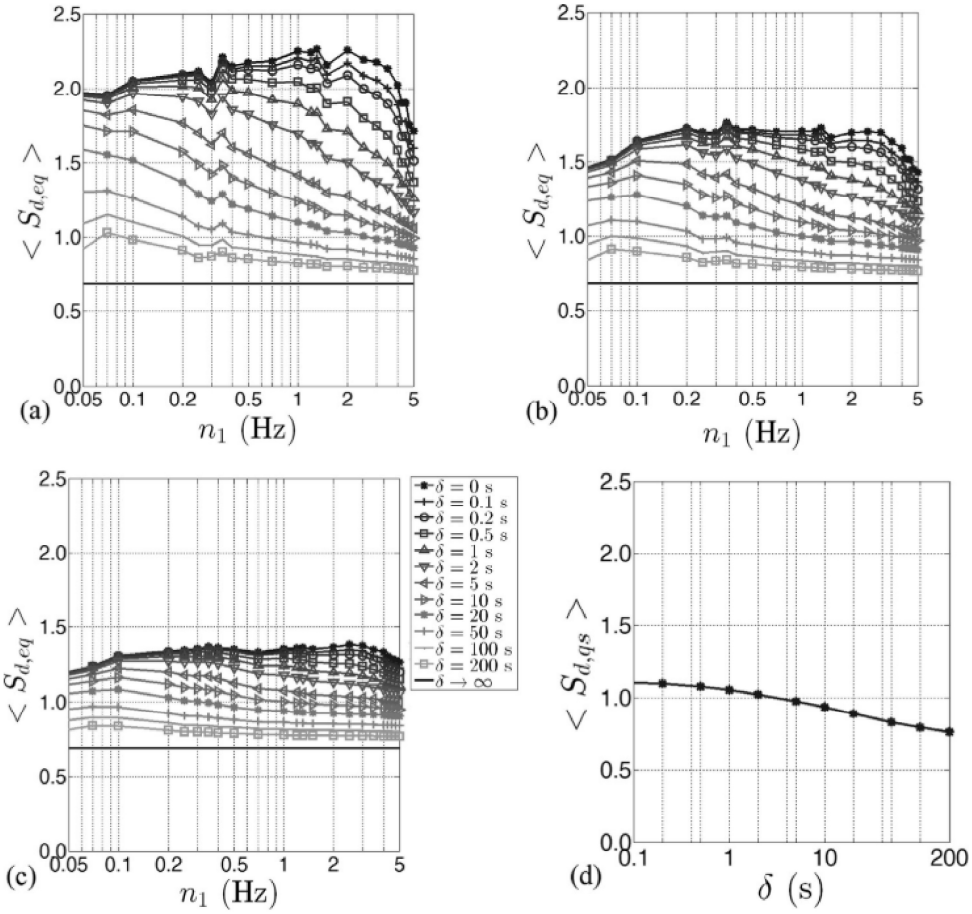

Fig. 5.1 Mean value of the equivalent response spectrum: (a) $\xi = 0.002$; (b) $\xi = 0.01$; (c) $\xi = 0.05$;(d) quasi-static solution. (From Solari and De Gaetano (2018))

Although the development of the TRS method required the collection of several wind speed time histories and a step-by-step procedure, its application is very straightforward. This makes it one of the few candidates for the future codification of design approaches against thunderstorm outflow winds.

The TRS method has some limitations and scope for improvements. It is developed by adopting the classical method of decomposition for the wind speed and thus the crosswind part of wind speed is not considered, which makes it applicable only to alongwind response calculation. It is also developed using thunderstorm wind speed time histories collected in a

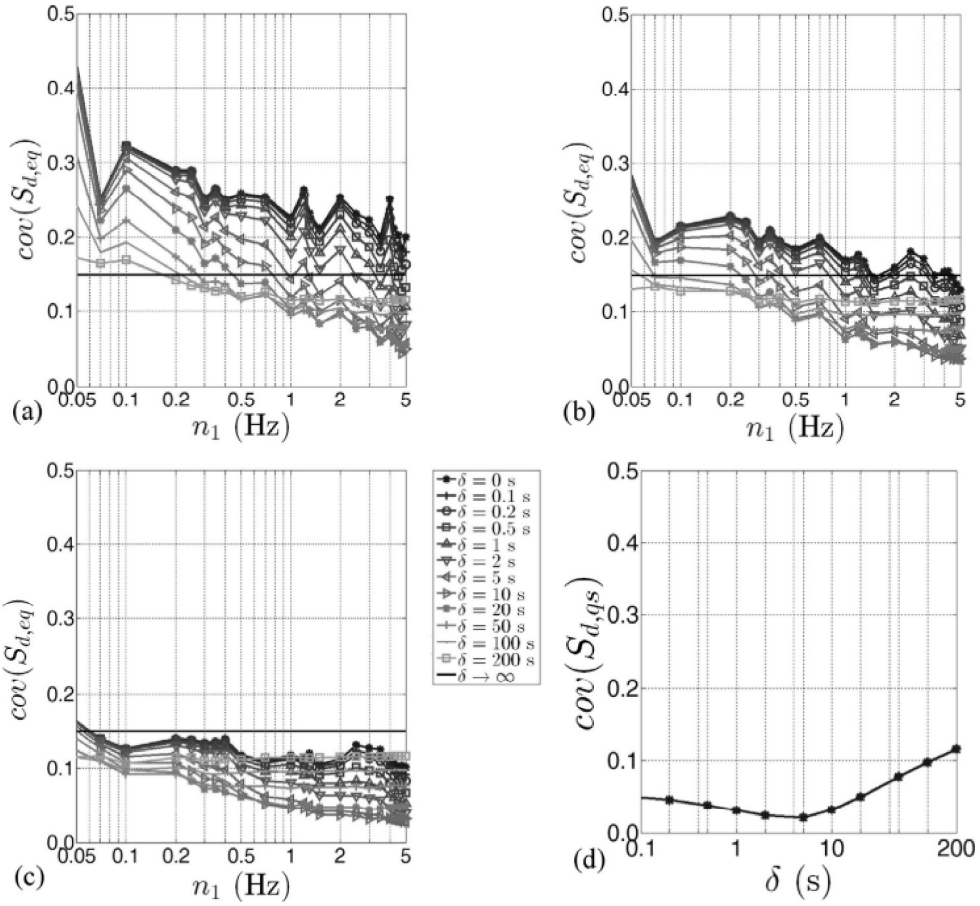

Fig. 5.2 Cov of the equivalent response spectrum: (a) $\xi = 0.002$; (b) $\xi = 0.01$; (c) $\xi = 0.05$; (d) quasi-static solution. (From Solari and De Gaetano (2018))

specific geographical location so its applicability to other geographical locations with different roughness, terrain, and homogeneity should be studied. However, this requires the collection of thunderstorm wind speed data in different geographical locations.

The thunderstorm response spectrum curves presented in Solari and De Gaetano (2018) are reproduced in this paper using the same input of the 93 wind speed records, for validation of accuracy. Fig. 5.5 shows the reproduced mean of equivalent TRS. Comparison of the reproduced equivalent TRS with the one in Solari and De Gaetano (2018) shows that there is a slight difference between the two in the low-frequency region of lowly damped systems with $\xi = 0.002$. To investigate the sources of error, the source code for the generation of the TRS in Solari and De Gaetano (2018) was studied and it was found that the process of solving the equation of motion using discrete Fourier transform in the frequency domain had some limitations for lowly damped low-frequency systems. It is known that solving the equation of motion in the frequency

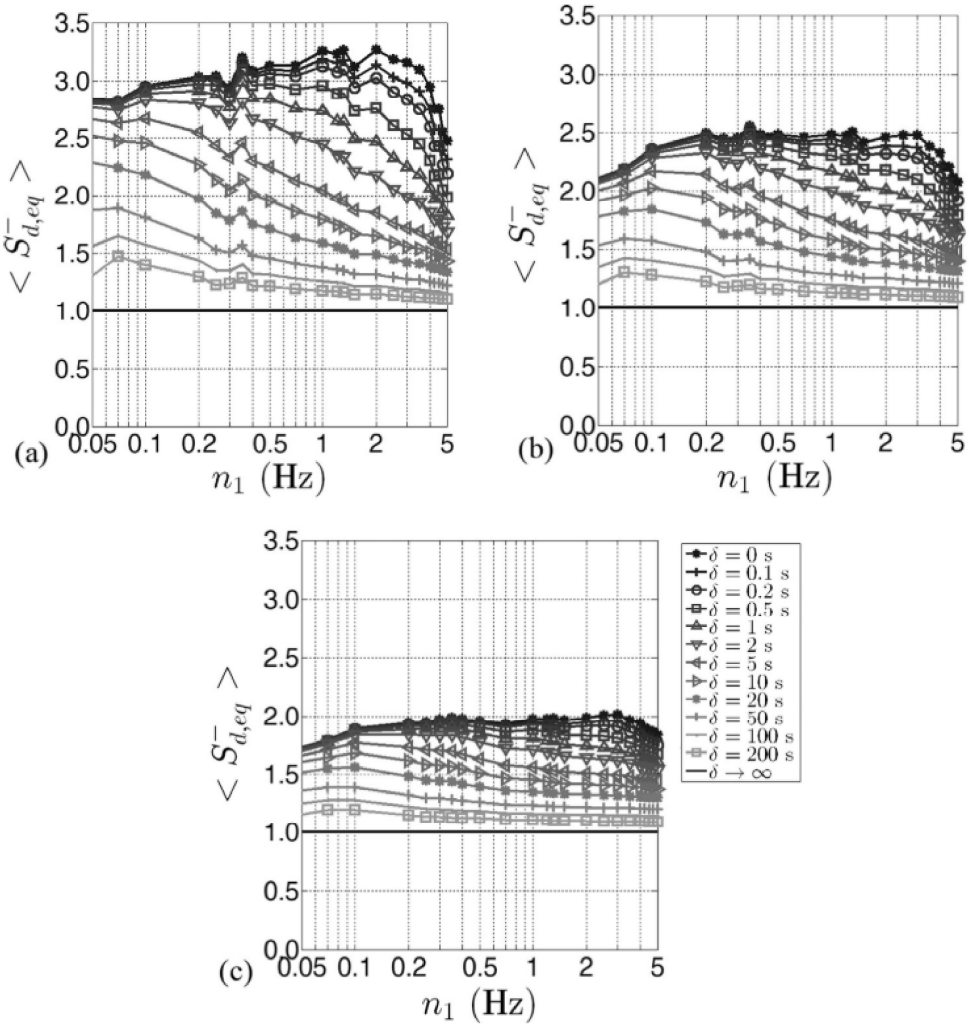

Fig. 5.3 Mean value of the equivalent "mean" response spectrum: (a) $\xi = 0.002$; (b) $\xi = 0.01$; (c) $\xi = 0.05$. (From Solari and De Gaetano (2018))

domain requires the addition of a sufficient length of zeros at the end of the time history of the excitation and this is especially more important for lowly damped low-frequency systems where the vibration requires a longer time to be damped (Chopra, 2014; Clough and Penzien, 2003). The provision of insufficient length of zeros in solving the equation of motion in the frequency domain was found to be the source of error. Thus, the TRS in Solari and De Gaetano (2018) needs slight improvement in the region of lowly damped, low-frequency systems to correct the inaccuracy introduced while solving the equation of motion in the frequency domain. The reproduction of the TRS was done by solving the equation of motion in the time domain and thus, the result presented in Fig. 5.5 do not have the explained inaccuracy.

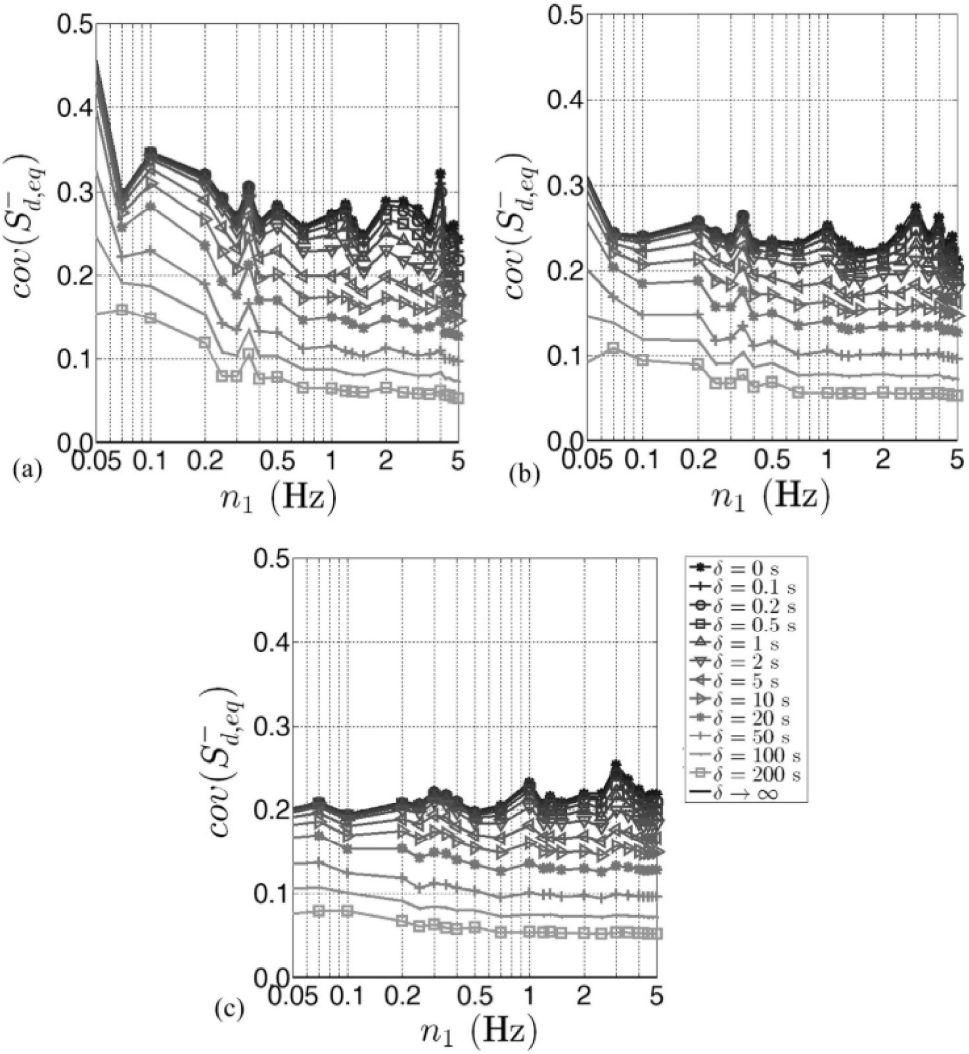

Fig. 5.4 Cov of the equivalent "mean" response spectrum: (a) $\xi = 0.002$; (b) $\xi = 0.01$; (c) $\xi = 0.05$. (From Solari and De Gaetano (2018))

Similarly, the mean value of the equivalent "mean" response spectrum shown in Solari and De Gaetano (2018) (Fig. 5.3) also needs some improvement in the case of low-frequency and lowly-damped systems. It was corrected and reproduced in Fig. 5.6.

5.2.2 Validation of the TRS method using two case studies of downbursts

In this section, validation of the TRS method using full-scale monitoring data during two case studies of downbursts is presented. The full-scale monitoring consisted of a 16.6 m high slender lighting pole that has been continuously registering simultaneous measurements of wind speed

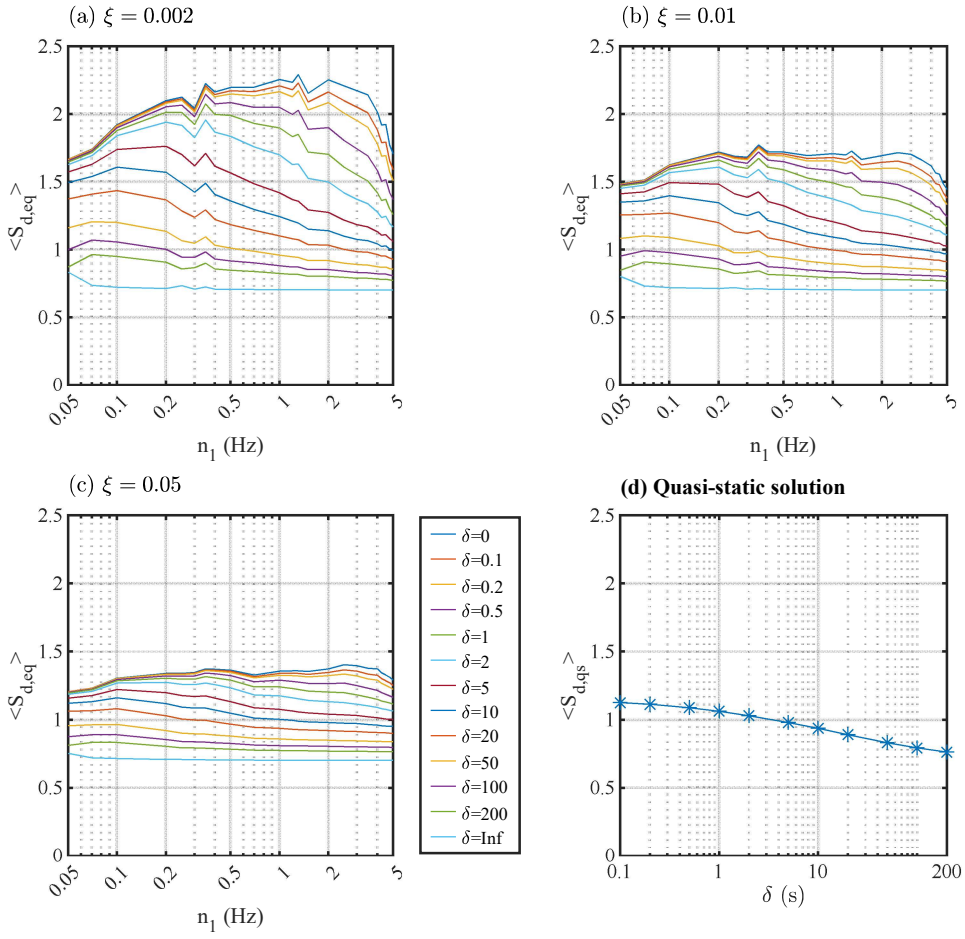

Fig. 5.5 Mean value of the equivalent response spectrum: (a) $\xi = 0.002$; (b) $\xi = 0.01$; (c) $\xi = 0.05$; (d) quasi-static solution.

and structural response data. Two case studies of downbursts that are registered by the monitoring system and introduced in Chapter 3 were selected for validation.

The TRS method was applied for the calculation of the peak top displacement of the full-scale monitored structure during the selected two case studies of downbursts with the aim of comparing the outcomes of the TRS method and the registered peak top displacement of the structure. As discussed in the previous section, the response spectrum is a factor that multiplies either the 30-second moving averaged mean or the 1-second peak static response to obtain the peak dynamic response. In this application, the equivalent "mean" response spectrum, $S^{-}_{d,eq}$, that multiplies the mean static response to obtain the peak dynamic response is intended to be used. Initially, a MATLAB function that gives $S^{-}_{d,eq}$ for any given input of size factor, δ,

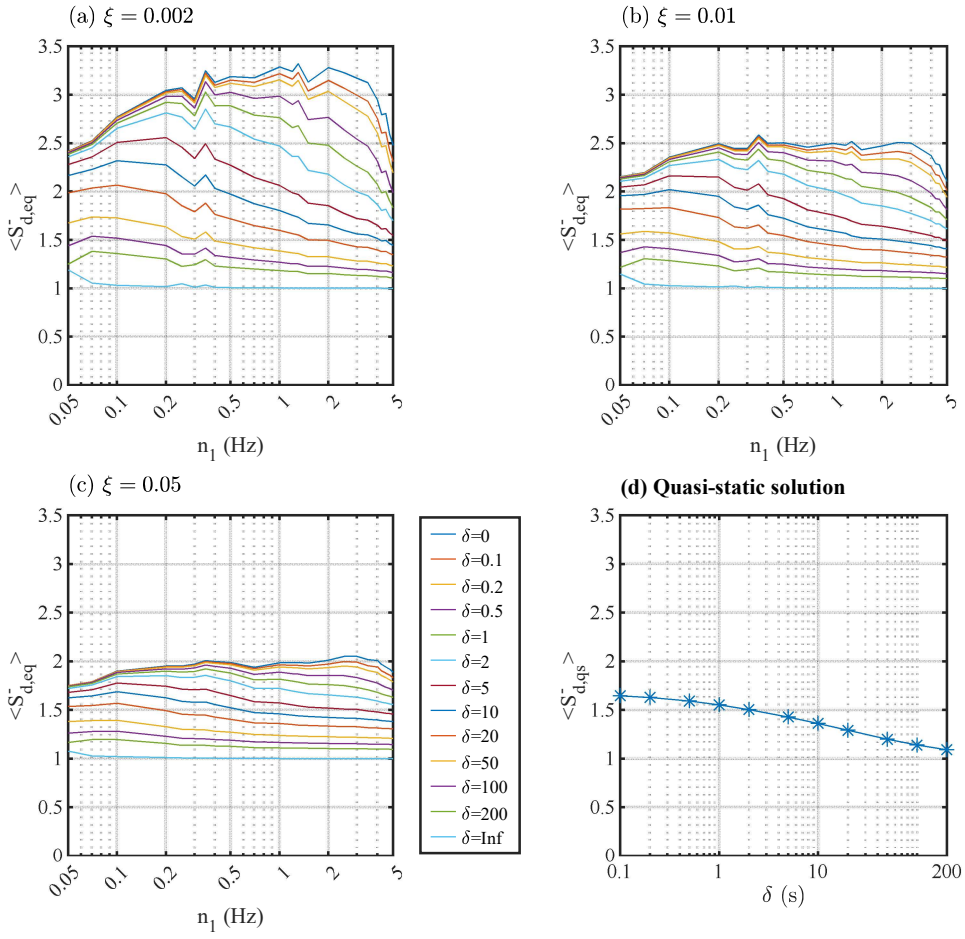

Fig. 5.6 Mean value of the equivalent "mean" response spectrum: (a) $\xi = 0.002$; (b) $\xi = 0.01$; (c) $\xi = 0.05$;(d) quasi-static solution.

natural frequency, n_1, and damping ratio, ξ_1, was written using the 93 thunderstorm wind records previously used for the development of the thunderstorm response spectrum curves (Solari, 2016; Solari and De Gaetano, 2018; Solari et al., 2015b). This was done to avoid the manual reading and interpolation of the response spectrum curves and for future extension to an online portal.

The analysis was intended to be done considering the first bending mode. The first bending modes of the monitored structure in the two principal directions X and Y are at natural frequencies of 0.85 Hz and 0.75 Hz respectively. These axes are rotated by 44.5 degrees in the counterclockwise direction from the East-North direction. However, the wind speed during the two case studies was not directed toward either of the two principal axes of bending. Thus, the wind speed obtained from the anemometer in the East and North directions referred to as $u_E(t,h)$

Table 5.1 Size factor δ calculated for the two case studies

Event	δ_X	δ_Y
Apr 04, 2019	4.81	2.96
Oct 02, 2019	3.49	5.95

and $u_N(t,h)$ respectively were projected on the principal axes of the structure (Eqs. 5.20 and 5.21), denoted as X and Y and estimation of the response spectrum value was done separately in the X and Y directions.

$$u_X(t,h) = u_E(t,h)\cos 44.5 + u_N(t,h)\sin 44.5 \tag{5.20}$$

$$u_Y(t,h) = -u_E(t,h)\sin 44.5 + u_N(t,h)\cos 44.5 \tag{5.21}$$

Although the first mode damping ratio of the monitored structure, ξ_1, was estimated using operational modal analysis techniques, values of 0.2%, 0.5%, and 1% were considered to address its uncertainty (Chapter 2).

The size factor, δ, which is a parameter in the application of the TRS method is calculated in the X and Y direction separately following the procedure explained in Chapter 4. Regarding the input parameters for the calculation of the size factor, the following considerations are made.

The exponential decay coefficient of alongwind fluctuating wind, c_{uz}, in the vertical direction was considered as 10 following the recommendation in Solari and Piccardo (2001) for ABL wind field. The power coefficient of the modal shape in the two principal bending directions, $\zeta_{1,X} = 1.6$ and $\zeta_{1,Y} = 1.9$, were considered according to the dynamic property of the structure investigated in Chapter 2. The height of the structure, H, is 16.6 m. To calculate $\bar{u}_{max,i}$ in the X and Y direction, first the time-varying mean wind speeds in the two principal directions, $\bar{u}_X$ and $\bar{u}_Y$, were obtained by extracting the running mean wind speeds over a moving 30-second window from u_X and u_Y. Consecutively, $\bar{u}_{max,X}(h)$ and $\bar{u}_{max,Y}(h)$ were identified as the mean wind speeds in the X and Y direction at the instant of maximum resultant wind speed. The maximum mean wind speeds at the equivalent height of the structure, $\bar{u}_{max,X}(z_{eq})$ and $\bar{u}_{max,Y}(z_{eq})$, were calculated by applying the empirical formula for the vertical profile of the mean wind speed proposed in Wood et al. (2001). In this empirical formula, the parameter Z_{max} which is the height of the maximum wind speed is considered as 25 m. Although this parameter is uncertain, a comparison not presented here showed that its overall effect on the value of δ for the considered case studies is small (δ increases by $\approx$5% when $Z_{max} = 100$ m is considered instead of $Z_{max} = 25$). The size factor δ calculated for the two case studies of downbursts in the X and Y direction is presented in Table 5.1.

Table 5.2 $S_{d,eq}^{-}$ calculated for the two case studies

Event	$\xi = 0.2\%$		$\xi = 0.5\%$		$\xi = 1\%$	
	X	Y	X	Y	X	Y
Apr 04, 2019	2.14	2.36	1.93	2.11	1.80	1.94
Oct 02, 2019	2.29	2.07	2.04	1.88	1.89	1.75

The equivalent "mean" response spectrum, $S_{d,eq}^{-}$, in the X and Y directions were obtained using the three input parameters, δ, n, and ξ (Table 5.2). To avoid the introduction of uncertainty due to other structural and aerodynamic parameters while calculating the mean response, the comparison was done on the peak displacement of the structure obtained as a product of the mean registered displacement and $S_{d,eq}^{-}$. Thus, the time-varying mean top displacements of the structure in the X and Y directions, $\bar{X}(t)$ and $\bar{Y}(t)$, were extracted from the registered top displacement by calculating the moving average over 30 seconds. The peak dynamic response in the two principal directions, $\hat{X}$ and $\hat{Y}$ were calculated as a product of $S_{d,eq}^{-}$ and the maximum value of the registered time-varying mean top displacements of the structure, $\bar{X}_{max}$ and $\bar{Y}_{max}$. For ease of comparison, Fig. 5.8 shows the calculated resultant peak top displacement using the TRS method represented by horizontal lines and the time history of the registered resultant top displacement in the 10-minute duration centering the maximum wind speed.

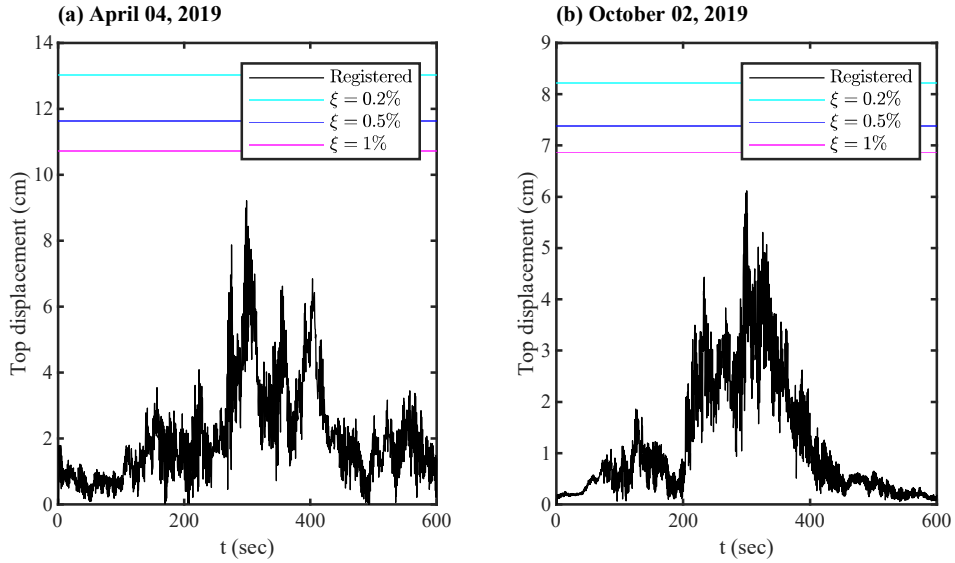

Fig. 5.7 Comparison of top displacement calculated with TRST and the registered top displacement

It can be clearly seen from Fig. 5.7 that the peak top displacement calculated using the TRS method is higher than the registered top displacement for both case studies of downburst

Table 5.3 Percentage difference [%] between registered top displacement and calculated using TRST

Event	$\xi = 0.2\%$	$\xi = 0.5\%$	$\xi = 1\%$
Apr 04, 2019	41	26	16
Oct 02, 2019	34	21	12

events. The difference is quantified in Table 5.3 as a percentage difference between the calculated and registered top displacement for all assumptions of damping. The percentage differences range between 41% and 12% indicating that, for the considered structure, the thunderstorm response spectrum method was able to predict the peak response with a slight overestimation. The overestimation can be attributed to the fact that the TRS values are the mean of the values obtained using several thunderstorm wind speed time histories.

5.3 Generalized gust front factor (G-GFF) method

5.3.1 Background

Gust front factor is a framework introduced in Kwon and Kareem (2009). It generalizes the gust loading approach, which is widely used in design codes for the wind load calculation of ABL winds, under the same framework as the wind load calculation of downbursts/thunderstorms. This method introduced four factors that take into account variation in the vertical profile of wind speed, dynamic effects due to the sudden rise in wind speed, nonstationarity of turbulence, and transient aerodynamics. The product of the four factors gives the gust front factor which reduces to the gust loading factor in the case of ABL winds. To make this framework applicable to any design code/standard, the generalized gust front factor (G-GFF) was introduced in Kwon and Kareem (2013). The G-GFF which is a product of an equivalent mean peak factor and RMS of the fluctuating response has an analogous definition to the gust response factor in ABL winds. In addition, a closed-form solution for the RMS of the fluctuating response and the mean peak factor was given assuming a long pulse duration storm (Kwon and Kareem, 2013, 2019).

The definition of the generalized gust front factor and the closed-form solution of the RMS of the fluctuating response was given in Kwon and Kareem (2009), Kwon and Kareem (2013), and Kwon and Kareem (2019). However, for a better evaluation of the considered assumptions and to lay a better foundation for a detailed comparison with the TRS method, the derivation of the G-GFF is presented in this section. More specifically, the RMS of the fluctuating response whose closed form solution is given (Kwon and Kareem, 2009, 2013, 2019) is derived in this

section to better understand the fundamental assumptions behind the result and to identify points of improvement.

In this method, the wind speed is considered as a summation of time varying-mean wind speed component, $\bar{u}(z,t)$, and a nonstationary fluctuating component, $u'(z,t)$.

$$u(z,t) = \bar{u}(z,t) + u'(z,t) \tag{5.22}$$

The time-varying mean wind speed is modeled as a product of normalized time function, $\bar{u}(t)$, and a height-dependent mean wind speed, $\bar{u}(z)$.

$$\bar{u}(z,t) = \bar{u}(t)\bar{u}(z) \tag{5.23}$$

The normalized time-varying function is defined as:

$$\bar{u}(t) = sin\left(\frac{\pi}{t_d}t\right) \tag{5.24}$$

where t_d is the pulse duration of the excitation.

The vertical profile of the mean wind speed was modeled adopting the formulation proposed in Vicroy (1991) and Vicroy (1992).

$$\bar{u}(z) = a\bar{U}_{max}\alpha(z) \tag{5.25}$$

where $a = 1.345$ and $\bar{U}_{max}$ is the maximum wind speed at Z_{max}:

$$\alpha(z) = \left[e^{-0.22(z/Z_{max})} - e^{-2.75(z/Z_{max})}\right] \tag{5.26}$$

The nonstationary fluctuating component of the wind speed is modeled as:

$$u'(z,t) = c_1\bar{u}(z,t)\tilde{u}'(z,t) \tag{5.27}$$

where c_1 is an amplitude-modulating coefficient that plays the role of constant turbulence intensity, I_u, and $\tilde{u}'(z,t)$ is a normalized stationary Gaussian process of the fluctuating component with zero mean and unit standard deviation. The turbulence intensity defined in ASCE 7-05 (2005) for different terrain exposure was adopted in Kwon and Kareem (2009) for gust fronts and it is given by:

$$c_1 = c\left(\frac{10}{0.6H}\right)^{1/6} \tag{5.28}$$

where c is a constant for arbitrary terrain exposures (ASCE 7-05, 2005) and H is the structure's height.

$$c = \begin{cases} 0.3 & for \quad ExposureB \\ 0.2 & for \quad ExposureC \\ 0.15 & for \quad ExposureD \end{cases} \tag{5.29}$$

With the assumption of the strip and quasi-steady theory, the aerodynamic force per unit height is given by:

$$f(z,t) = \frac{1}{2}\rho BC_d[u(z,t)]^2 \tag{5.30}$$

where ρ is the density of air; B is the width of the structure; and C_d is the drag coefficient.

Substituting Eq. 5.22 for the wind speed and assuming small turbulence, Eq. 5.30 becomes:

$$f(z,t) = \frac{1}{2}\rho BC_d\bar{u}^2(t)\bar{u}^2(z) + \rho BC_d c_1\bar{u}^2(t)\bar{u}^2(z)\tilde{u}'(z,t) \tag{5.31}$$

Thus, similar to the definition of the wind speed, the force per unit length also has a time-varying mean component, $\bar{f}(z,t) = \frac{1}{2}\rho BC_d\bar{u}^2(t)\bar{u}^2(z)$, and a non-stationary fluctuating component, $f'(z,t) = \rho BC_d c_1\bar{u}^2(t)\bar{u}^2(z)u'(z,t)$.

Response to the time-varying mean force

From Eq. 5.31, the time-varying mean force is given by:

$$\bar{f}(z,t) = \frac{1}{2}\rho BC_d\bar{u}^2(t)\bar{u}^2(z) \tag{5.32}$$

The generalized 1^{st} mode mean force is:

$$\bar{f}_1(t) = \int_0^H \bar{F}(z,t)\psi_1(z)dz \tag{5.33}$$

where $\psi_1(z)$ is the first mode shape which was approximated as linear (z/H) in Kwon and Kareem (2013).

The quasi-static response at the top of the structure is:

$$\bar{x}_{st}(t) = \frac{\bar{f}_1(t)}{K} \tag{5.34}$$

where K is the stiffness.

Substituting Eq. 5.32 and Eq. 5.33 in Eq. 5.34,

$$\bar{x}_{st}(t) = \frac{1}{K}\int_0^H \frac{1}{2}\rho B C_d \bar{u}^2(t)\bar{u}^2(z)\psi_1(z)dz \tag{5.35}$$

Substituting for $\bar{u}^2(z)$ from Eq. 5.25

$$\bar{x}_{st}(z,t) = \psi_1(z)\frac{1}{K}0.5\rho B C_d \bar{u}^2(t)[a\bar{U}_{max}]^2 \times \int_0^H [\alpha(z)]^2\psi_1(z)dz \tag{5.36}$$

The maximum quasi-static response at the top of the structure occurs when $\bar{u}^2(t) = 1$.

$$\bar{x}_{st} = \frac{1}{K}0.5\rho B C_d \bar{u}^2(t)[a\bar{U}_{max}]^2 \int_0^H [\alpha(z)]^2\psi_1(z)dz \tag{5.37}$$

The maximum dynamic displacement at the top of the structure due to the time-varying mean force can be defined using the pulse dynamic factor, I_2 introduced in Kwon and Kareem (2009) as:

$$max[\bar{x}_1(t)] = \bar{x}_{st} I_2 \tag{5.38}$$

I_2 is a pulse dynamic factor that takes care of the dynamic amplification due to the time-varying mean force (Kwon and Kareem, 2009). It is defined as the ratio of the maximum dynamic response due to the time-varying mean force over the maximum quasi-static response due to the time-varying mean force.

Consequently, the maximum dynamic response of the structure due to the time-varying mean force at various heights can be calculated as:

$$max[\bar{x}(z,t)] = \bar{x}_{st} I_2 \psi_1(z) = \bar{x}_{st}(z) I_2 \tag{5.39}$$

Response to the non-stationary fluctuating force

From Eq. 5.31, the non-stationary fluctuating force per unit height is:

$$f'(z,t) = \rho B C_d c_1 \bar{u}^2(t)\bar{u}^2(z)\tilde{u}'(z,t) \tag{5.40}$$

The generalized 1^{st} mode fluctuating force is

$$\begin{aligned} f_1'(t) &= \int_0^H f'(z,t)\psi(z) \\ &= \int_0^H \rho B C_d c_1 \bar{u}^2(t)\bar{u}^2(z)\tilde{u}'(z,t)\psi_1(z)dz \\ &= \rho B C_d c_1 \bar{u}^2(t)\int_0^H \bar{u}^2(z)\tilde{u}'(z,t)\psi_1(z)dz \end{aligned} \tag{5.41}$$

Substituting Eq. 5.25,

$$f_1'(t) = \rho B C_d c_1 \bar{u}^2(t)[a\bar{U}_{max}]^2 \int_0^H \alpha^2(z)\tilde{u}'(z,t)\psi_1(z)dz \tag{5.42}$$

The fluctuating wind speed is considered as a uniformly modulated stationary process and a long pulse duration storm is assumed in Kwon and Kareem (2009). This simplifies the definition of the power spectral density (PSD) of the generalized 1^{st} mode force and results in a PSD that is uniformly modulated in time. Furthermore, additional simplification was introduced because Davenport's spectrum (Davenport, 1967a), which is height-invariant, was considered for the PSD of the normalized stationary wind speed component.

The power spectral density of the normalized stationary zero mean wind speed, $S_{\tilde{u}'}(z,n)$, is:

$$S_{\tilde{u}'}(z,n) = \sqrt{S_{\tilde{u}'}(z_1,n)}\sqrt{S_{\tilde{u}'}(z_2,n)}Coh(y_1,y_2,z_1,z_2,n) \tag{5.43}$$

where $Coh(y_1,y_2,z_1,z_2,n)$ is the coherence function defined as (Davenport, 1967b; Simiu and Scanlan, 1996):

$$Coh(y_1,y_2,z_1,z_2,n) = exp\left[-\frac{n\left[c_{uz}^2(z_1-z_2)^2 + c_{uy}^2(y_1-y_2)^2\right]^{1/2}}{U(10)}\right] \tag{5.44}$$

where $U(10)$ is the wind velocity at $z = 10\ m$ and it is considered as 20% of the maximum mean wind speed $\bar{U}_{max}$ in Kwon and Kareem (2009); c_{uz} and c_{uy} are exponential decay coefficients. Although the exponential decay coefficients were shown to be dependent on height, wind speed, and terrain (Simiu and Scanlan, 1996), it is customary to use an average value. Similarly, an average value of 6 was considered in Kwon and Kareem (2013).

With the assumptions and definitions described above, the power spectral density of the generalized 1^{st} mode fluctuating force is given by:

$$S_{f_1'}(t,n) = (\rho BC_d c_1)^2 \bar{u}^4(t)[a\bar{U}_{max}]^4 S_{\tilde{u}'}(n)\frac{1}{B^2}\int_0^H\int_0^H\int_0^B\int_0^B \alpha^2(z_1)\alpha^2(z_2)R_y(y_1,y_2,n) \\ R_z(z_1,z_2,n)\psi_1(z_1)\psi_1(z_2)dy_1dy_2dz_1dz_2 \tag{5.45}$$

where R_y and R_z are the coherence functions in the horizontal and vertical directions respectively.

The normalized Davenport spectrum adopted in Kwon and Kareem (2009) is defined in Davenport (1964) as

$$s_{\tilde{u}'}(n) = \frac{2}{3}\frac{x^2}{(1+x^2)^{4/3}}\frac{1}{n} \tag{5.46}$$

where $x = \frac{1200\cdot n}{U(10)}$; $U(10)$ is the mean wind speed at 10 meters height in m/s and n is the frequency in Hz.

$R_y(y_1,y_2,n)$ and $R_z(z_1,z_2,n)$ are defined as:

$$R_y(y_1,y_2,n) = exp\left(-\frac{c_{uy}n|y_1-y_2|}{U(10)}\right) \tag{5.47}$$

$$R_z(z_1,z_2,n) = exp\left(-\frac{c_{uz}n|z_1-z_2|}{U(10)}\right) \tag{5.48}$$

By defining $y_1' = y_1/B$, $y_2' = y_2/B$, $z_1' = z_1/H$, and $z_2' = z_2/H$, $dy_1 = dy_1'B$, $dy_2 = dy_2'B$, $dz_1 = dz_1'H$, $dz_2 = dz_2'H$, and noting that the mode shape is approximated as linear, $\psi_1(z_1) = z_1/H$ and $\psi_1(z_z) = z_2/H$, Eq. 5.45 can be redefined as:

$$S_{f_1'}(t,n) = (\rho BC_d I_u H)^2 \bar{v}^4(t)[a\bar{V}_{max}]^4 S_u'(n)\int_0^1\int_0^1\int_0^1\int_0^1 \alpha^2(z_1')\alpha^2(z_2')R_y(y_1',y_2',n) \\ R_z(z_1',z_2',n)z_1'z_2'dy_1'dy_2'dz_1'dz_2' \tag{5.49}$$

The integral yields the product of the joint acceptance functions in the horizontal and vertical directions, $|J_y(n)|^2$ and $|\tilde{J_z}(n)|^2$.

$$S_{f_1'}(t,n) = (\rho BC_d c_1 H)^2 \bar{v}^4(t)[aV_{max}^-]^4 S_u'(n)|J_y(n)|^2|\tilde{J_z}(n)|^2 \tag{5.50}$$

The joint acceptance functions are:

$$|J_y(n)|^2 = \int_0^1 \int_0^1 R_y(y_1', y_2', n) dy_1' dy_2' \tag{5.51}$$

$$|\tilde{J}_z(n)|^2 = \int_0^1 \int_0^1 \alpha^2(z_1')\alpha^2(z_2') R_z(z_1', z_2', n) z_1' z_2' dz_1' dz_2' \tag{5.52}$$

The solution to $|J_y(n)|^2$ is given in Davenport (1967a) by defining $R_y(y_1, y_2, n) = exp(-D)$, where $D = exp\left(\frac{c_{uy} n |y_1 - y_2|}{U(10)}\right)$ and solving the integral numerically. The result is reproduced in Fig. 5.8 as a function of D and as indicated in Davenport (1967a), the integral can be approximated by the equation

$$|J_y(n)|^2 = \frac{1}{1 + 0.5D} \tag{5.53}$$

Similar solution is given for the $|J_y(n)|^2$ in Kwon and Kareem (2013) as

$$|J_y(n)|^2 = \frac{1}{1 + 0.5 c_{uy} \frac{nB}{U(10)}} \tag{5.54}$$

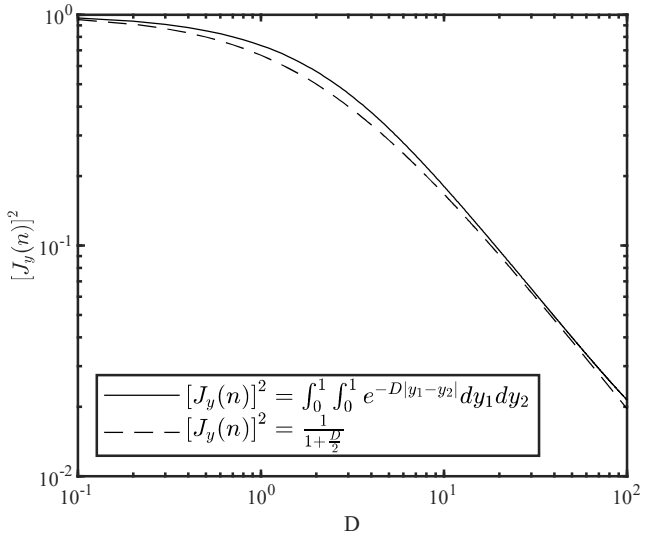

Fig. 5.8 Joint acceptance function in the horizontal direction

The exact solution of $|\tilde{J}_z(n)|^2$ is dependent on the ratio of z_{max}/H because of the coupling between the coherence of the wind field in the vertical direction and the mean wind speed profile. However, although it is not explicitly stated, the dependency of $|\tilde{J}_z(n)|^2$ on the mean

wind speed profile is neglected in Kwon and Kareem (2013) by separating $\alpha(z_1')\alpha(z_2')z_1'z_2'$ from the integral of the coherence function and redefining $|\tilde{J}_z(n)|^2 = (CA)^2|J_z(n)|^2$, where $|J_z(n)|^2 = \int_0^1\int_0^1 R_z(z_1',z_2',n)z_1'z_2'dz_1'dz_2'$ and

$$(CA)^2 = \int_0^1\int_0^1 \left[e^{-0.22Hz_1'/Z_{max}} - e^{-2.75Hz_1'/Z_{max}}\right]^2 \left[e^{0.22Hz_2'/Z_{max}} - e^{-2.75Hz_2'/Z_{max}}\right]^2 z_1'z_2'dz_1'dz_2' \tag{5.55}$$

Thus, Eq. 5.50 is modified as:

$$S_{f_1'}(t,n) = (\rho BC_d c_1 H)^2 \bar{u}^4(t)[a\bar{U}_{max}]^4 S_u'(n)(CA)^2|J_y(n)|^2|J_z(n)|^2 \tag{5.56}$$

It should be noted that there is a slight difference in the definition of $(CA)^2$ given above and the one in Kwon and Kareem (2013) and Kwon and Kareem (2019).

The solution to $|J_z(n)|^2$ is given in Kwon and Kareem (2013) as:

$$|J_z(n)|^2 = \frac{1}{1 + c_3 c_{uz}\frac{nH}{U(10)}} \tag{5.57}$$

where c_3 is a height-dependent polynomial approximation introduced in Kwon and Kareem (2013) as a matrix multiplication for different exposure class

$$c_3 = \begin{bmatrix} 1.370 & -2.036 & 1.097 & 0.199 \\ 2.184 & -2.853 & 1.324 & 0.198 \\ 1.364 & -2.722 & 1.408 & 0.206 \\ 3.145 & -4.630 & 1.819 & 0.204 \end{bmatrix} \begin{bmatrix} 10^{-9}H^3 \\ 10^{-6}H^2 \\ 10^{-3}H \\ 1 \end{bmatrix} \begin{matrix} A \\ B \\ C \\ D \end{matrix} \tag{5.58}$$

Fig. 5.9 shows the comparison between the joint acceptance function calculated using the formulation given by Eq. 5.57 (in black) and the exact solution obtained through numerical integration for different assumptions of Z_{max}/H. It can be observed that the approximation of the joint acceptance function given by Eq. 5.57 is not highly variable with the terrain class it is close to the exact solution. However, from the derivation, the height and terrain dependency of the newly introduced parameter c_3 is not clear.

The power spectral density of the generalized 1^{st} mode response due to the nonstationary fluctuating component of wind speed is:

$$\begin{aligned} S_{x_1'}(t,n) =& |H(n)|^2 S_{F_1'}(t,n) \\ S_{x_1'}(t,n) =& |H(n)|^2(\rho BC_d c_1 H)^2 \bar{u}^4(t)[a\bar{U}_{max}]^4 (CA)^2 S_{\tilde{u}'}(n)|J_y(n)|^2|J_z(n)|^2 \end{aligned} \tag{5.59}$$

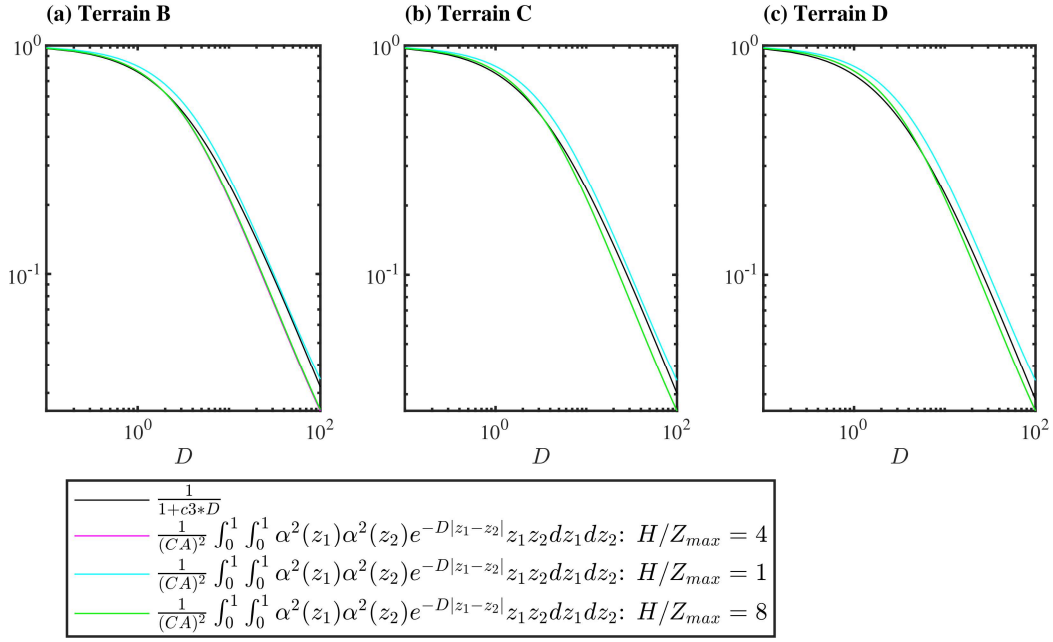

Fig. 5.9 Joint acceptance function in the vertical direction

where $H(n)$is the mechanical admittance of the structure.

$$|H(n)|^2 = \frac{1}{K^2}\frac{1}{\left(1-\frac{n^2}{n_0^2}\right)^2+4\xi^2\frac{n^2}{n_0^2}} \tag{5.60}$$

The RMS of the generalized 1^{st} mode fluctuating response is:

$$\begin{aligned}\sigma_{x_1'}(t) &= \sqrt{\int_0^\infty S_{x_1'}(t,n)dn} \\ &= \rho BC_d c_1 H\bar{u}^2(t)[a\bar{U}_{max}]^2(CA)\sqrt{\int_0^\infty |H(n)|^2 S'_{\tilde{u}}(n)|J_y(n)|^2|J_z(n)|^2dn} \\ &= \rho BC_d c_1 H\bar{u}^2(t)[a\bar{U}_{max}]^2(CA)\sqrt{B'+R'}\end{aligned} \tag{5.61}$$

The integral in this equation which is the area under the normalized power spectral density curve multiplied by the square of the mechanical admittance and the joint acceptance functions is approximated as having a background, B', and, R', resonant components. The background component, which is the area excluding the resonant peak can be approximated as:

$$\begin{aligned} B' &= \int_0^{n_0-\delta} |H(0)|^2 S_{\tilde{u}'}(n)|J_y(n)|^2|J_z(n)|^2 dn \\ &= \frac{1}{K^2}\int_0^{n_0-\delta} S_{\tilde{u}'}(n)|J_y(n)|^2|J_z(n)|^2 dn \end{aligned} \tag{5.62}$$

Davenport (1967a) defined the reduced frequency as nH/U_{10} and stated that B' can be found from the force spectrum (which does not include the resonant peak) by treating the joint acceptance as a "high-frequency cut-off" at a reduced frequency of 3/8. A reduced frequency of 3/8 is considered as, the frequency at which the joint acceptance becomes significantly small. Thus, Eq. 5.62 becomes:

$$B' = \frac{1}{K^2}\int_0^{\frac{3V_{10}}{8H}} S_{\tilde{u}'}(n)dn \tag{5.63}$$

Substituting Eq. 5.46 for $S_{\tilde{u}'}(n)$ and integrating, B' is becomes:

$$B' = \frac{1}{K^2}\left[1 - \frac{1}{\left[1+\left(\frac{3}{8}\frac{1200}{H}\right)^2\right]^{1/3}}\right] \tag{5.64}$$

The resonant component, which is the area under the resonant peak, can be approximated as:

$$R' = \int_{n_1-\delta}^{n_1+\delta} |H(n_1)|^2 S_{\tilde{u}'}(n_1)|J_y(n_1)|^2|J_z(n_1)|^2 dn \tag{5.65}$$

This integral can be simplified as (Simiu and Scanlan, 1996):

$$R' = \frac{\pi n_1}{4\xi_1 K^2} S_{\tilde{u}'}(n_0)|J_y(n_1)|^2|J_z(n_1)|^2 \tag{5.66}$$

where ξ_1 is the first mode damping ratio and n_1 is the first mode natural frequency.

Substituting B' and R', Eq. 5.63 becomes

$$\sigma_{x_1'}(t) = \frac{1}{K}\rho B C_d c_1 H \bar{u}^2(t)[a\bar{U}_{max}]^2(CA)\sqrt{B+R} \tag{5.67}$$

$$B = 1 - \frac{1}{\left[1+\left(\frac{3}{8}\frac{1200}{H}\right)^2\right]^{1/3}} \tag{5.68}$$

$$R = \frac{\pi n_1}{4\xi_1} S_{\tilde{u}'}(n_1)|J_y(n_1)|^2|J_z(n_1)|^2 \tag{5.69}$$

The RMS of the fluctuating response at various heights can be found as:

$$\sigma_{x'}(z,t) = \sigma_{x'_1}(t)\psi_1(z) \tag{5.70}$$

Substituting Eq. 5.67 into Eq. 5.70

$$\sigma_{x'}(z,t) = \left[\frac{1}{K}\rho BC_d c_1 H \bar{u}^2(t)[a\bar{U}_{max}]^2(CA)\sqrt{B+R}\right]\psi_1(z) \tag{5.71}$$

The RMS of the fluctuating response in Kwon and Kareem (2013) is presented as height invariant and this is a correct definition if it is intended to calculate the maximum fluctuation at the top of the structure.

The maximum value of the RMS of the fluctuating response occurs when $\bar{u}^2(t)$ is equal to 1.

$$max[\sigma_{x'}(z,t)] = \left[\frac{1}{K}\rho BC_d c_1 H[a\bar{U}_{max}]^2(CA)\sqrt{B+R}\right]\psi_1(z) \tag{5.72}$$

Maximum response and generalized gust front factor

Neglecting the effect of translation of the storm, the total response of the structure is the summation of the time-varying mean component, $\bar{x}(z,t)$, and the non-stationary fluctuating component, $x'(z,t)$.

$$x(z,t) = \bar{x}(z,t) + x'(z,t) \tag{5.73}$$

Assuming the mean and fluctuating parts of the response will attain a maximum value at the same instant, the maximum response can be approximated as:

$$max[x(z,t)] \approx max[\bar{x}(z,t)] + max[x'(z,t)] \tag{5.74}$$

Adopting a similar definition as in the case of ABL winds, the fluctuating response is defined as a product of the mean peak factor, g, and the RMS of the fluctuating response, $g \cdot \sigma_x(z,t)$ Kwon and Kareem (2013). Thus,

$$max[x(z,t)] \approx max[\bar{x}(z,t)]\left[1 + \frac{g \cdot max[\sigma_{x'}(z,t)]}{max[\bar{x}(z,t)]}\right] \tag{5.75}$$

The peak factor, which is time-varying for nonstationary processes, was simplified as time-invariant in (Kwon and Kareem, 2013) by applying Michaelov's approach of finding an equivalent stationary process of equivalent time interval T_{eq} whose peak value is similar to the non-stationary process under consideration (Michaelov et al., 2001). It was defined in (Kwon and Kareem, 2019) as:

$$g = \sqrt{2ln(v_0 T_{eq})} + \frac{0.5772}{\sqrt{2ln(v_0 T_{eq})}} \tag{5.76}$$

where v_0 is the time-dependent cyclic rate. T_{eq} was approximated as $0.37t_d$ for a long pulse duration.

Substituting Eq. 5.39 to Eq. 5.76,

$$max[x(z,t)] = \bar{x}_{st}(z) I_2 \left[1 + \frac{g \cdot max\left[\sigma_{x'}(z,t)\right]}{\bar{x}_{st}(z) I_2}\right] \tag{5.77}$$

Defining the generalized gust front factor, $G_{G,G-F}$, analogously with the gust response factor in ABL winds as a factor that multiplies the static response due to the mean wind force to obtain the peak dynamic response:

$$max[x(z)] = \bar{x}_{st}(z) \cdot G_{G,G-F} \tag{5.78}$$

$$G_{G,G-F} = \left[1 + \frac{g \cdot max[\sigma_{x'}(z,t)]}{\bar{x}_{st}(z) I_2}\right] I_2 \tag{5.79}$$

Substituting Eqs. 5.39 and 5.72, $G_{G,G-F}$ becomes,

$$G_{G,G-F} = \left[1 + \frac{g c_1 H(CA)\sqrt{B+R}}{0.5 I_2 \int_0^H [\alpha(z)]^2 \psi_1(z) dz}\right] I_2 \tag{5.80}$$

The factor I_2 takes a value greater than 1. It was evaluated for a range of pulse duration values, t_d, fundamental frequency, n_1, and damping ratio, ξ_1, and is shown in Fig. 5.10. In general, I_2 is less than 1.1 for $t_d > 50$ *sec* or for $n_1 > 0.25$ *Hz*. The mean storm duration calculated from the recorded 93 thunderstorms in Solari et al. (2015a) was 248 seconds and as a result, I_2 can safely be assumed as 1 for most applications.

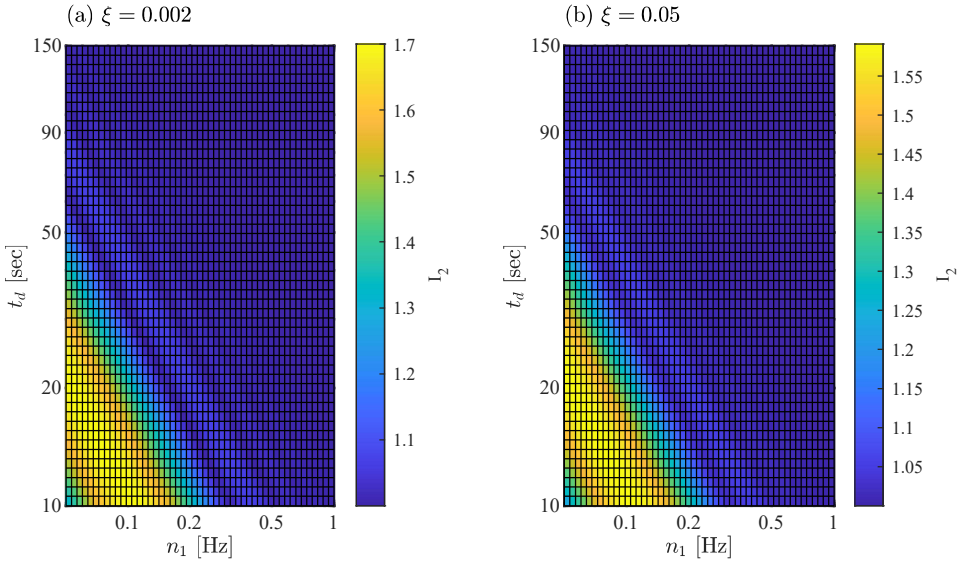

Fig. 5.10 Variability of the pulse dynamic factor, I_2, with pulse duration, t_d, and natural frequency, n

5.3.2 Validation of the G-GFF method using the two case studies of downbursts

In this section, the generalized gust front factor method is applied for the calculation of the peak response of the monitored structure during the two case studies of downbursts introduced in Section 5.2.2, with the aim of comparing the outcomes of the G-GFF method and the registered top displacement of the structure. It should be recalled that the generalized gust front factor,$G_{G,G-F}$, is a factor that multiplies the mean static response to obtain the peak dynamic response.

Similar to the validation of the TRS method, the validation of the G-GFF method is also intended to be done considering the first bending mode. For the same reason given in Section 5.2.2, the estimation of the G-GFF was done separately in the X and Y directions considering natural frequencies of 0.85 Hz and 0.75 Hz respectively.

The following considerations were made for the input parameters of the G-GFF calculation using 5.80. Since the wind was coming from the direction of the sea during both events, terrain category D was considered according to the definition of ASCE 7-05 (2005). The pulse duration of the storm, t_d, was calculated according to the procedure presented in Solari et al. (2015a). It was found to be 158 sec and 160 sec for the events of April 04, 2019, and October 02, 2019, respectively. Consequently, the pulse dynamic factor I_2 was considered as unity. The model by Vicroy (1991) was used to calculate the maximum mean wind speed, $\bar{u}_{max,i}$, in the X and

Table 5.4 $G_{G,G-F}$ calculated for the two case studies

Event	$\xi = 0.2\%$		$\xi = 0.5\%$		$\xi = 1\%$	
	X	Y	X	Y	X	Y
Apr 04, 2019	1.98	2.11	1.90	1.96	1.87	1.90
Oct 02, 2019	2.06	1.94	1.94	1.88	1.89	1.86

Y directions from the maximum mean wind speed at the anemometric height in the X and Y directions. The parameter, Z_{max}, which is the height of the maximum wind speed, is considered as 25 m. Although this parameter is uncertain, for the considered case studies, its overall effect on the value of the generalized gust front factor was verified to be small ($G_{G,G-F}$ decreases by a maximum of $\approx$6% when $Z_{max} = 100$ m is considered instead of $Z_{max} = 25$). In addition, since the structure is slender with small width, the correlation of the wind field in the horizontal direction was assumed to be perfect, i.e. the joint acceptance function in the horizontal direction, $|J_y(n)|^2$, is assumed to be 1.

The generalized gust front factor, $G_{G,G-F}$, in the X and Y directions, were obtained using the described input parameters and it is presented in Table 5.4. To avoid the introduction of uncertainty due to other structural and aerodynamic parameters while calculating the mean response, the comparison was done on the peak displacement of the structure obtained as a product of the mean registered displacement and $G_{G,G-F}$. Thus, the time-varying mean component of the registered top displacements of the structure in the X and Y directions, $\bar{X}(t)$ and $\bar{Y}(t)$, were obtained by calculating the moving average over 30 seconds. The peak response in the X and Y direction, $\hat{X}$ and $\hat{Y}$ were calculated as a product of $G_{G,G-F}$ and the maximum value of time-varying mean top displacement of the structure, $\bar{X}_{max}$ and $\bar{Y}_{max}$. For ease of comparison, Fig. 5.11 shows the time history of the resultant registered peak top displacement in the 10-minute duration centering the maximum wind speed (in black) and the calculated resultant peak top displacements represented by horizontal lines.

From Fig. 5.11, it can be observed that the peak top displacement calculated using the G-GFF method is higher than the registered top displacement for both case studies of downburst events. The difference is quantified in Table 5.5 as a percentage difference between the calculated and registered top displacement for all assumptions of damping. The percentage difference ranges between 27% and 15% indicating that, for the considered structure, the generalized gust front factor method was able to predict the peak response calculation with a slight overestimation.

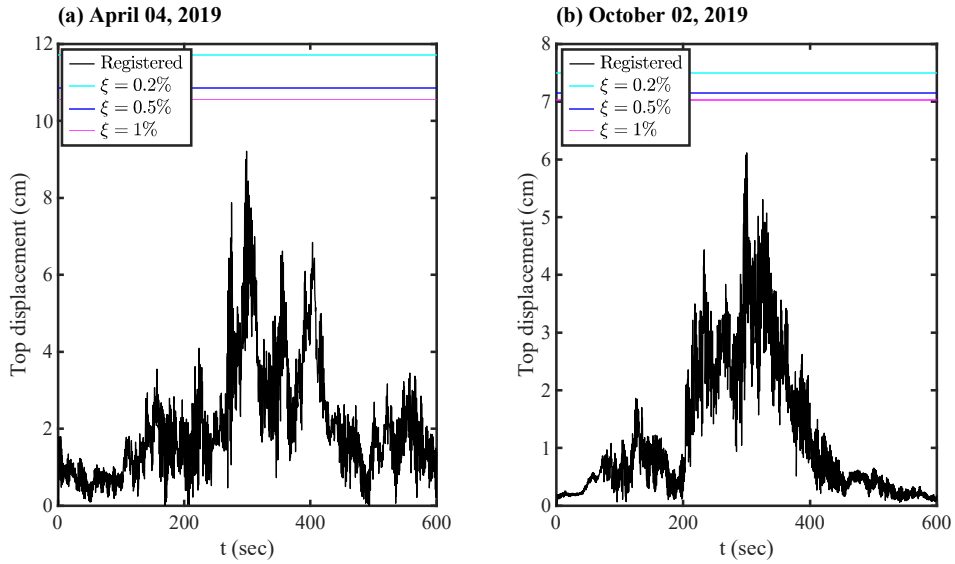

Fig. 5.11 Comparison of top displacement calculated with the G-GFF method and the registered top displacement

Table 5.5 Percentage difference [%] between registered top displacement and calculated using G-GFF method

Event	$\xi = 0.2\%$	$\xi = 0.5\%$	$\xi = 1\%$
Apr 04, 2019	27	18	15
Oct 02, 2019	23	17	15

5.4 Comparison between the G-GFF and TRS methods

The generalized gust front factor method and thunderstorm response spectrum method are considered in this study because of their potential for the codification of the design of structures against downbursts. Although the development of the thunderstorm response spectrum technique required numerous wind speed data records during downbursts, its application is straightforward. Similarly, the derivation of the gust front factor was rather complex but its application is through the calculation of the generalized gust front factor, $G_{G,G-F}$, which is a simple expression given in Eq 5.80. In this section, the theoretical basis of the two approaches is critically compared highlighting their sources of uncertainties. Furthermore, the gust response factors resulting from the two methods for structures with varying dynamic properties and size is compared.

In both approaches, the wind speed is modeled as the sum of a time-varying mean component and fluctuating component (Eq. 5.1 and Eq. 5.22). In the case of the TRS method, the time function for the time-varying mean component was extracted from each of the 93 input wind

speed time histories using a moving window of 30 seconds (Eq. 5.4), and in the case of the G-GFF method it was represented by a half-sin function (Eq. 5.24).

In both methods, the fluctuating component is modeled as a product of the time-varying standard deviation and a normalized stationary fluctuating component of unit standard deviation. However, in the case of the TRS method, the time-varying standard deviation is extracted from each of the 93 input wind speed time histories over a moving window of 30-second and the time-varying turbulence intensity is obtained as the ratio of the time-varying standard deviation to the time-varying mean wind speed. While in the case of the G-GFF, the time-varying standard deviation is considered to be similar to the time function of the mean wind speed multiplied by a constant value of turbulence intensity (Eq. 5.27).

The turbulence intensity is a governing parameter in the G-GFF method and its uncertainty was shown to influence the $G_{G,G-F}$ by a higher magnitude (Kwon and Kareem, 2019). The definition of turbulence intensity for ABL winds is adopted in Kwon and Kareem (2009) and it is dependent on the height of the structure and the terrain class (Eq. 5.27). In the TRS method, the turbulence intensity was considered to be varying with time but constant along the height. Thus, both of the methods can be improved with further field monitoring data of turbulence intensity especially its height-varying properties during downburst events. In addition, the correlation between turbulence intensity and terrain roughness in downburst winds should also be investigated.

The normalized fluctuating component, $\tilde{u}'(z,t)$, is treated to have similar spectral properties as ABL winds in both approaches. In the case of the TRS method, the normalized fluctuating component at the anemometric height was extracted from the 93 input wind speed time histories, and its variability in height was considered by replacing the time history at the anemometric height with an equivalent perfectly correlated turbulent fluctuation using the equivalent wind spectrum technique (Solari, 1988) (Eq. 5.6). In the case of the G-GFF method, the normalized Davenport spectrum that is height independent was considered for $\tilde{u}'(z,t)$ (Davenport, 1967a), and the coherence functions of ABL wind with exponential decay coefficients obtained from literature were considered (Eq. 5.44 and Eq. 5.46).

In the derivation of the G-GFF method, the partial correlation of the wind field in the horizontal and vertical directions is considered. In contrast, in the TRS method, the wind field is considered to be perfectly correlated in the horizontal direction while it is partially correlated in the vertical direction.

In the G-GFF method, the vertical profile of the mean wind speed is modeled through the empirical equation given in Vicroy (1991) and Vicroy (1992) and consideration of other models such as Wood et al. (2001) for the vertical profile is not applicable because the closed-form

solution of the RMS of the fluctuating response given in Kwon and Kareem (2013, 2019) is derived adopting this vertical profile (Eq. 5.26). On the other hand, the TRS method leaves the choice of the vertical profile of the mean wind speed to the user, as the derivation did not involve the vertical profile of the mean wind speed (Eq. 5.19).

Both the TRS method and G-GFF methods consider MDOF systems whose 1^{st} mode shape can be defined by a single expression. These structures are identified as a generalized single degree of freedom systems in structural dynamics (Chopra, 2014; Clough and Penzien, 2003). Consequently, only the first mode response is considered in both methods. The first mode shape is modeled as a linear mode shape, z/H, in the G-GFF method and as a power function, $(z/H)^{\zeta}$ in the TRS method with the possibility of defining the power coefficient, ζ, by the user.

In the TRS method, the response was calculated by solving the equation of motion in the time domain while in the case of the G-GFF method, the response to the fluctuating wind force was treated in the frequency domain. The response to the fluctuating wind force was considered to be the product of the mean equivalent peak factor and the RMS of the fluctuating response. Closed-form solutions are given for both the mean peak factor and the RMS of the fluctuating response.

Both methods give a factor that multiplies the mean static load/response to get the peak dynamic load/response and this factor is classically referred to as "the gust response factor" in ABL winds. In the following, "the gust response factor" defined as $G_{G,G-F}$ in the G-GFF method and defined as $S^{-}_{d,eq}$ in the TRS method is compared graphically by plotting the value of $G_{G,G-F}$, calculated considering several assumptions explained below, and the equivalent "mean" thunderstorm response spectrum, $S^{-}_{d,eq}$, calculated using the 93 thunderstorm records, on a single graph. To make the comparison on a similar basis, the following considerations are made.

- Vicroy's model was used for the mean wind profile in both methods.
- Since the TRS method is developed considering the perfect correlation of the turbulent wind field in the horizontal direction, the joint acceptance function in the horizontal direction, $|J_y(n)|^2$, in the application of the G-GFF method was considered as unity.
- The exponential decay coefficient of the coherence function in the vertical direction, c_{uz}, was considered as 6 in both methods.
- The storm duration in the G-GFF method was considered as 286 seconds because the mean storm duration of the 93 thunderstorm records was 286 seconds.
- The pulse dynamic factor, I_2, was considered as unity.

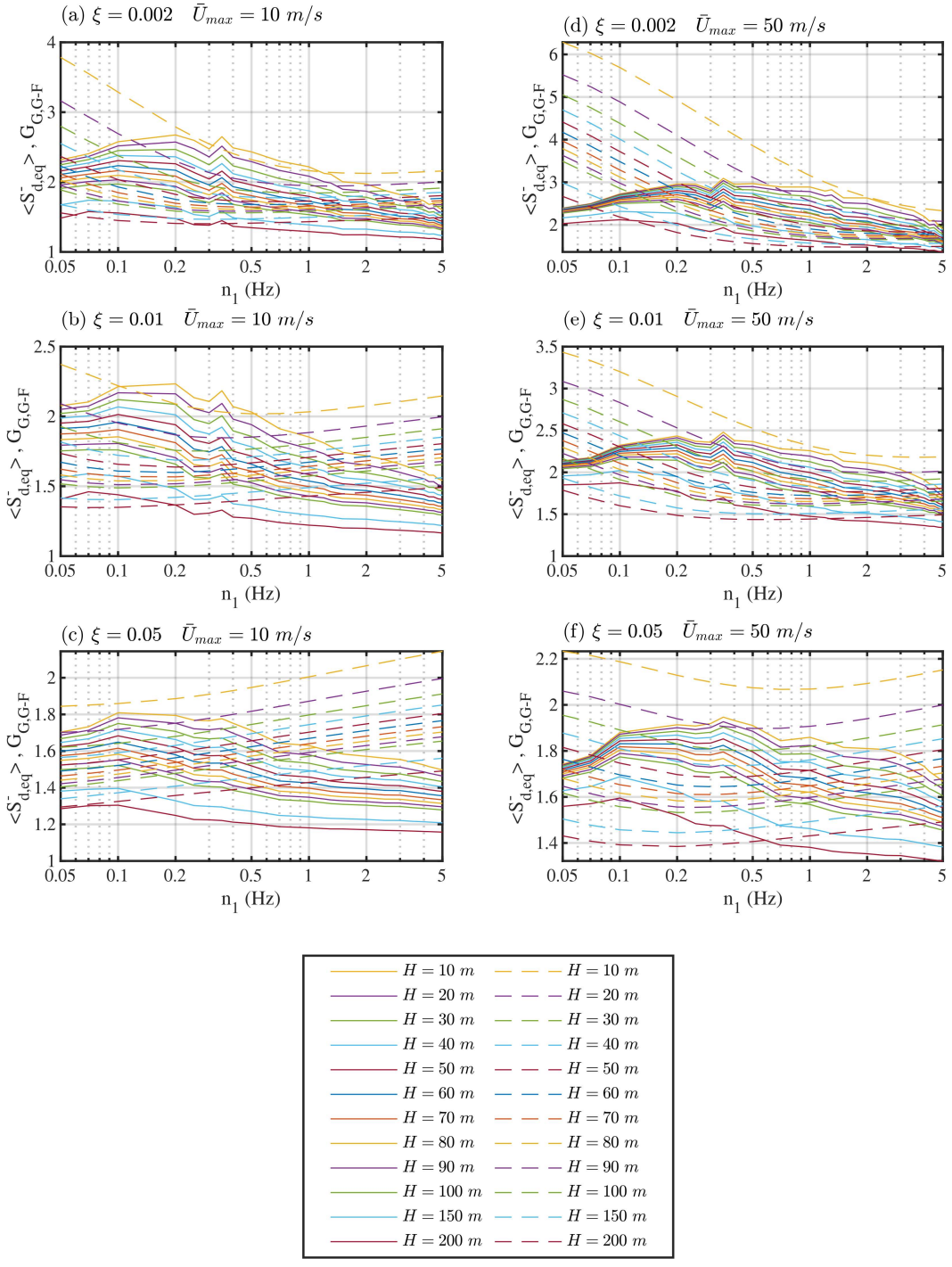

Fig. 5.12 Comparison between results of the gust response factor calculated using TRS method (solid line) and G-GFF method (broken line) assuming terrain class D

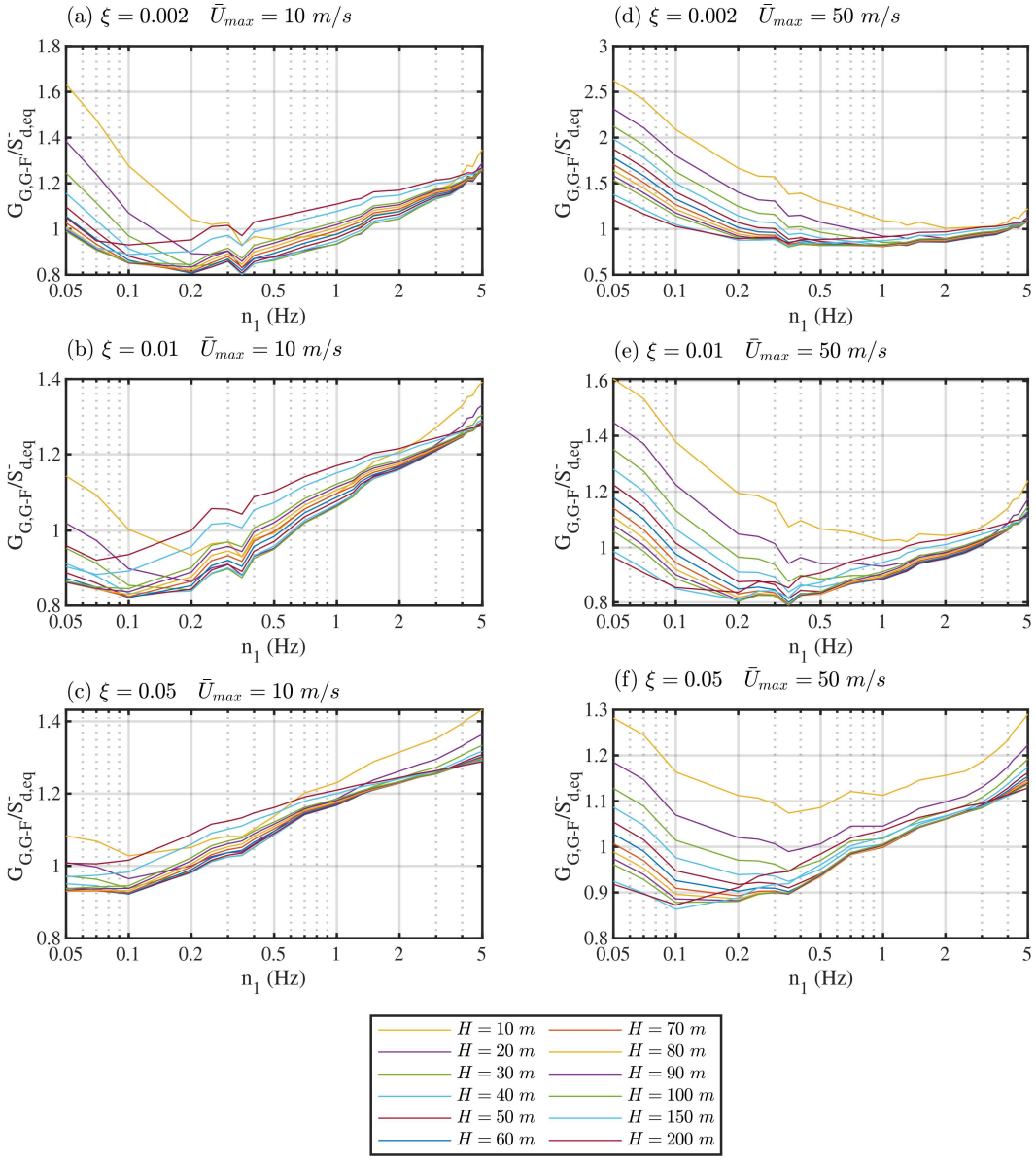

Fig. 5.13 Ratio of $G_{G,G-F}$ and $S^{-}_{d,eq}$ assuming terrain class D

Fig. 5.12 shows the gust response factor obtained using the G-GFF method, $G_{G,G-F}$, (in broken line) and TRS method, $S^{-}_{d,eq}$, (in solid line) for the terrain class of D, assuming $U_{max} = 10\ m/s$ (a-c) and $U_{max} = 50\ m/s$ (d-f). Comparing Fig. 5.12(a-c) with Fig. 5.12(d-f), both of the response factors $S^{-}_{d,eq}$ and $G_{G,G-F}$ increase as the maximum wind speed increases. This is expected because the turbulent wind becomes highly correlated as the wind speed increases. Focusing on the trend of $S^{-}_{d,eq}$ and $G_{G,G-F}$ with fundamental frequency, except for very low-frequency region, $S^{-}_{d,eq}$ has a decreasing trend with fundamental frequency regardless of the

damping ratio and U_{max}. For lowly damped systems with $\xi = 0.002$, the $G_{G,G-F}$ decreases as the fundamental frequency increases. However, this trend is reversed for highly damped systems with $\xi = 0.05$ where there is a slight increase in the $G_{G,G-F}$ with increasing natural frequency.

Fig. 5.13 shows the ratio of $G_{G,G-F}$ to $S^{-}_{d,eq}$ shown in Fig. 5.12. For $U_{max} = 10\ m/s$ (Fig. 5.13(a-c)), the ratio ranges from $\approx$ 0.8 - 1.6, and for $U_{max} = 50\ m/s$ (Fig. 5.13(d-f)), the ratio ranges from $\approx$ 0.8 - 2.6. It can be noted that for low fundamental frequency systems, the ratio increases with an increase in U_{max} while the ratio decreases with an increase in U_{max} for high fundamental frequency system. In comparison, $G_{G,G-F}$ is notably larger than $S^{-}_{d,eq}$ for lowly-damped low-frequency systems.

It should be noted that $G_{G,G-F}$ increases by a factor of 4/3 and 2 respectively when terrain classes of C and B are considered (Eq. 5.29) while $S^{-}_{d,eq}$ remains the same because it is not dependent on the terrain class. Thus, the values of $G_{G,G-F}$ shown in Fig. 5.12 and the ratios shown in Fig. 5.13 will be shifted upwards and a remarkably higher gap between TRS method and G-GFF method will be observed when the terrain classes of C and B are considered.

Turbulence intensity is directly proportional to $G_{G,G-F}$ and it is considered as a terrain-dependent parameter given by Eq. 5.28 adopted from ASCE 7-05 (2005). To make the comparison between the TRS method and G-GFF methods on a closer assumption of turbulence intensity, the mean of the 10-minutes averaged turbulence intensity of the 93 thunderstorm records which is 0.12 was considered for the G-GFF method instead of that given by Eq. 5.28 and the comparisons made above were repeated. It should be noted that this will not make the assumptions of the turbulence intensity in the TRS method and G-GFF exactly the same because the turbulence intensity in the TRS method is time-varying while it is constant in G-GFF method. Fig. 5.14 reproduces the comparisons shown in Fig. 5.12 revising the results of the G-GFF method with a constant turbulence intensity of 0.12. Comparing $G_{G,G-F}$ in Fig. 5.14 with Fig. 5.12, it can be observed that the $G_{G,G-F}$ curves of various structure's heights are less dispersed when a constant turbulence intensity of 0.12 is considered rather than when a height-dependent constant turbulence intensity given by Eq. 5.28 is considered. This is expected because in the latter case, the turbulence intensity, and consequently the gust response factor increases with the height of the structure as the height decreases below $\approx$ 17 m and decreases with the height of the structure as the height increases above $\approx$ 17 m. This results in dispersed curves of gust response factor for different heights. Variability of the gust response factor with the height of structures is more evident in the case of the TRS method than the G-GFF method and this is attributed to the different models of vertical coherence of wind field used in the two methods.

Similarly, Fig. 5.15 reproduces the comparison shown in Fig. 5.13 revising the results of G-GFF with a constant turbulence intensity assumption. For $U_{max} = 10\ m/s$ (Fig. 5.15(a-c)), the ratio ranges from $\approx$ 0.8 - 1.4, and for $U_{max} = 50\ m/s$ (Fig. 5.15(d-f)), the ratio ranges from $\approx$

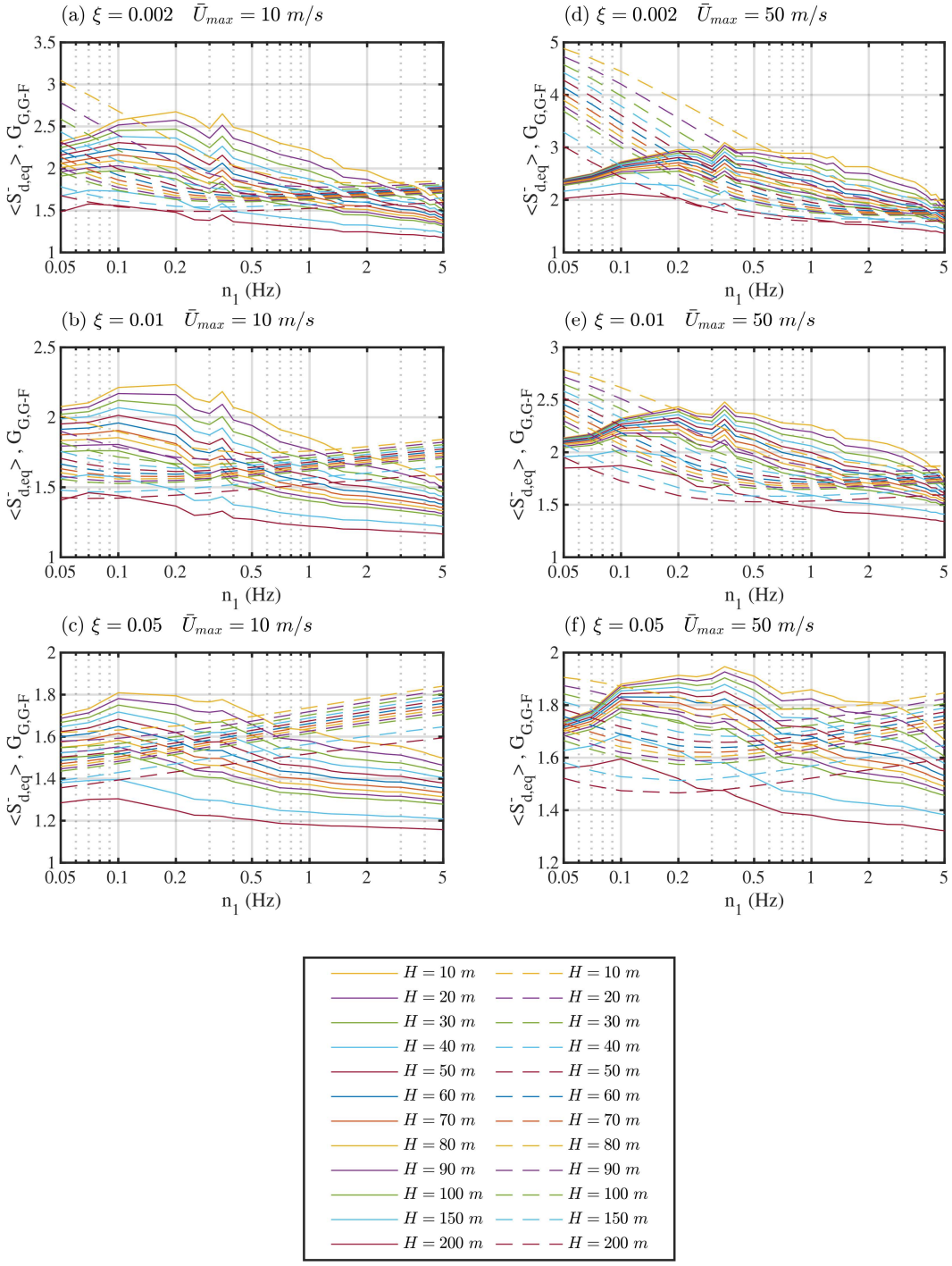

Fig. 5.14 Comparison between results of the gust response factor calculated using TRST (solid line) and G-GFF method (broken line) assuming terrain class D, and $I_u = 0.12$

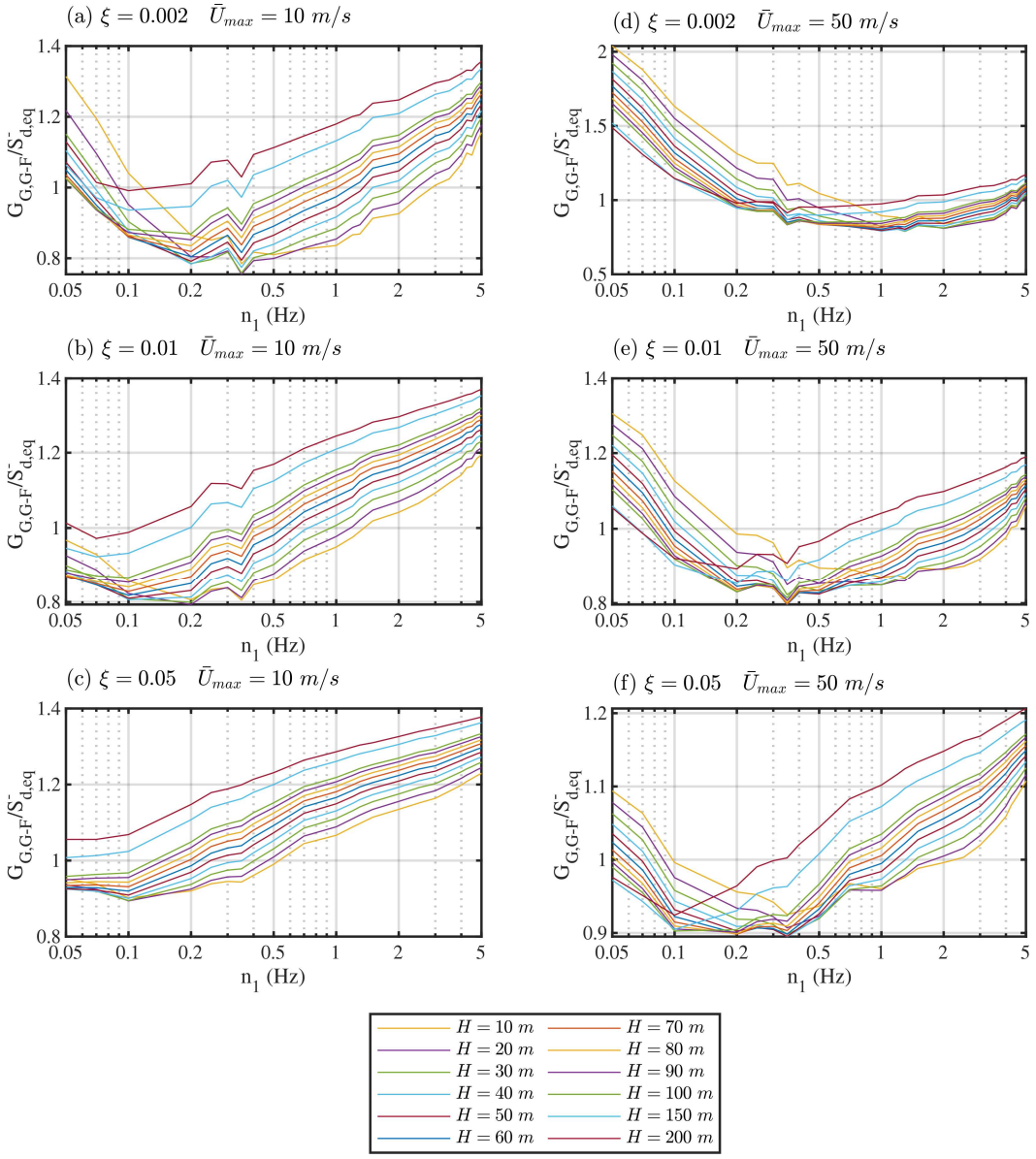

Fig. 5.15 Ratio of $G_{G,G-F}$ and $S^{-}_{d,eq}$ assuming terrain class D, and $I_u = 0.12$,

0.8 - 2 indicating a better match between the two methods when a constant turbulence intensity is considered in the G-GFF method. In comparison, $G_{G,G-F}$ is notably larger than $S^{-}_{d,eq}$ for lowly-damped low-frequency and highly-damped high-frequency systems. What is striking in this comparison is that in the range of fundamental frequencies of real slender structures ($n_1 = 0.1 - 1\ Hz$), the ratio between outputs of the two methods ranges between 0.8 and 2. This range is even closer (0.8-1.2) for the case where $U_{max} = 10\ m/s$. For most structure's heights, the

ratio is less than 1 indicating that the gust response factor calculated using the G-GFF method is lower than the TRS method.

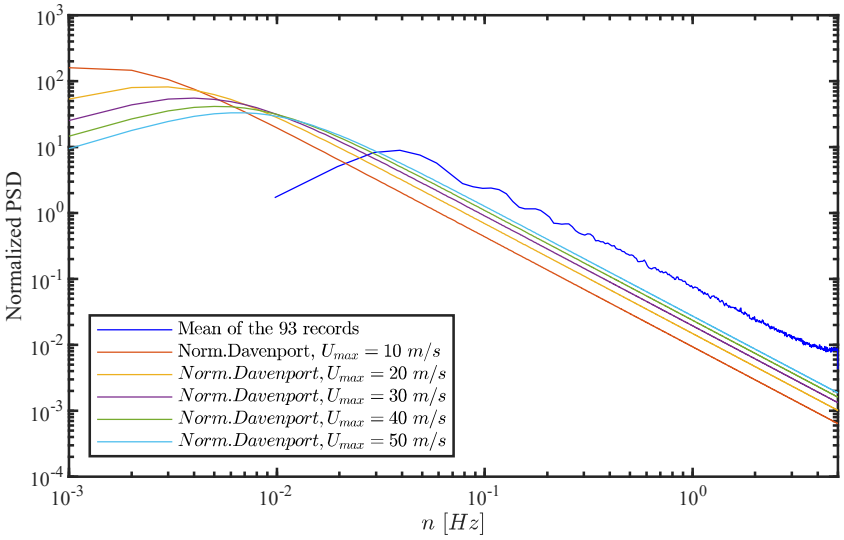

Fig. 5.16 Comparison between the PSD of the reduced fluctuating wind component of the 93 records and the normalized Davenport spectrum

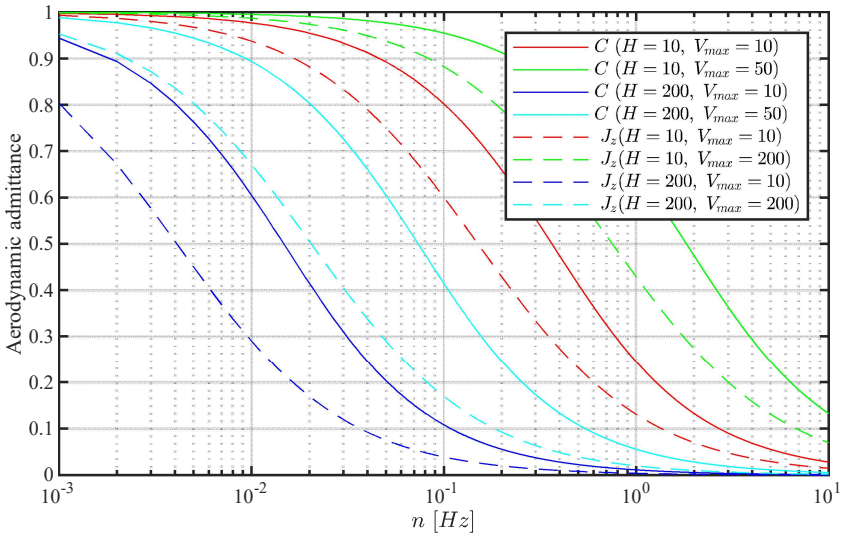

Fig. 5.17 Comparison between the aerodynamic admittance functions used in the TRS (solid lines) and in the G-GFF (broken lines) methods

To investigate the main sources of difference in the TRS method and G-GFF, the mean power spectral density of the reduced fluctuating component of wind speed of the 93 thunderstorm

records used in the TRS method was compared with the normalized Davenport power spectral density used in the G-GFF method and it is shown in Fig. 5.16. It should be noted that the normalized Davenport spectrum is dependent on the mean wind speed at 10 meters height, which is considered as 20% of U_{max} as recommended in Kwon and Kareem (2009). It is evident that the normalized Davenport spectrum has a similar shape to the PSD of the 93 thunderstorm records exhibiting a slight shift to the left. In the frequencies of interest for most structures ($0.1 - 1\ Hz$), the Davenport spectrum is lower than the PSD of the recorded thunderstorms. In addition, the Davenport spectrum decreases with U_{max}.

Another source of difference in the TRS and G-GFF methods is the aerodynamic admittance. In the TRS method, the frequency filter function, $C(n)$, defined in Eq. 5.28 plays the role of the joint acceptance function, $J_z(n)$, of the G-GFF defined in Eq. 5.25. Fig. 5.17 compares the two functions for various heights and maximum wind speeds. In all cases, it is evident that the joint acceptance function in the GFF method is significantly lower than its counterpart in the TRS method.

The comparison of the PSD of the normalized fluctuating component, as well as the joint acceptance function of the two methods, indicates that these two parameters can be the reason why the ratio of $G_{G,G-F}$ to $S^{-}_{d,eq}$ is less than 1 for some ranges of fundamental frequencies.

The mean peak factor formulation by Davenport, derived for stationary processes has been known to have an overestimation for lowly damped low-frequency systems (narrow band processes) (Vanmarcke, 1975). The mean peak factor employed in the G-GFF method which is based on Davenport's formulation can be the source of the notably high value of gust response factor in the G-GFF method for lowly damped low-frequency systems. A correction factor such as the one introduced in Roncallo et al. (2022) can be considered to rectify this overestimation.

The increasing trend of the gust factor in the G-GFF method with fundamental frequency for highly damped systems is not realistic but it could be because of the rising trend in the mean peak factor with frequency.

5.5 Conclusion

- The thunderstorm response spectrum (TRS) method and the generalized gust front factor (G-GFF) method are easily applicable methods for consideration in the codification of design procedures against downbursts.
- The thunderstorm response spectrum curves given in Solari and De Gaetano (2018) need some revision for the case of lowly damped, low-frequency systems.
- The applicability of the thunderstorm response spectrum curves given in Solari and De Gaetano (2018) in other geographical locations and terrain conditions should be studied.
- The definition of the joint acceptance function in the vertical direction in the G-GFF method as a terrain and height-dependent parameter needs some clarification and modification.
- The assumption of turbulence intensity as similar to ABL winds in the G-GFF method needs to be properly evaluated using monitoring data as it is directly proportional to the gust response factor.
- A comparison of the TRS and G-GFF showed that a better match can be obtained between the two methods when an approximately similar assumption of turbulence intensity is made, except for lowly-damped low-frequency systems and highly-damped high-frequency systems.
- The high value of the response factor in the G-GFF for lowly damped low-frequency systems could be attributed to the definition of the peak factor and that needs further investigation.
- Validation of the TRS and the G-GFF method using the response of the monitored structure during two case studies of the downburst showed that the two methods were able to predict the peak top displacement of the monitored structure in a range of 12-41% increase.
- Wind speed measurement data at various spatial coordinates is essential to improve the two analytical methods through data-driven turbulence and mean wind speed profile models.

References

ASCE 7-05 (2005). *Minimum Design Loads for Buildings and Other Structures*.

Brusco, S., Lerzo, V., and Solari, G. (2019). Directional response of structures to thunderstorm outflows. *Meccanica*, 54(9):1281–1306.

Brusco, S. and Solari, G. (2021). Transient aeroelasticity of structures subjected to thunderstorm outflows. *Eng. Struct.*, 245.

Chay, M. and Albermani, F. (2005). Dynamic Response of a SDOF System Subjected to Simulated Downburst Wind. *Proc. 6th Asia-Pacific Conf. Wind Eng.*

Chen, L. and Letchford, C. W. (2004a). A deterministic-stochastic hybrid model of downbursts and its impact on a cantilevered structure. *Eng. Struct.*, 26(5):619–629.

Chen, L. and Letchford, C. W. (2004b). Parametric study on the along-wind response of the CAARC building to downbursts in the time domain. *J. Wind Eng. Ind. Aerodyn.*, 92(9):703–724.

Chen, X. (2008). Analysis of Alongwind Tall Building Response to Transient Nonstationary Winds. *J. Struct. Eng.*, 134(5):782–791.

Choi, E. C. and Tanurdjaja, A. (2002). Extreme wind studies in Singapore. An area with mixed weather system. *J. Wind Eng. Ind. Aerodyn.*, 90(12-15):1611–1630.

Chopra, A. K. (2014). *Dynamics of Structures*. Pearson Education Limited, 4th edition.

Clough, R. W. and Penzien, J. (2003). *Dynamics of Structures, Third Edition*.

Davenport, A. G. (1964). The spectrum of horizontal gustiness near the ground in high winds. *J. R. Meteorol. Soc.*, 87:194–211.

Davenport, A. G. (1967a). Gust loading factors. *J. Struct. Div. Proc. Am. Soc. Civ. Eng.*, pages 11–34.

Davenport, A. G. (1967b). The Dependence of Wind Loads on Meteorological Parameters. In *Procceding Int. Res. Semin. Wind Eff. Biuldings Struct.*, pages 19–82.

Holmes, J., Forristall, G., and Mcconochie, J. (2005). Dynamic response of structures to thunderstorm winds. *10th Am. Conf. Wind Eng. ACWE 2005*, (July 2017).

Kwon, D. K. and Kareem, A. (2009). Gust-front factor: New framework for wind load effects on structures. *J. Struct. Eng.*, 135(6):717–732.

Kwon, D. K. and Kareem, A. (2013). Generalized gust-front factor: A computational framework for wind load effects. *Eng. Struct.*, 48:635–644.

Kwon, D. K. and Kareem, A. (2019). Towards codification of thunderstorm/downburst using gust front factor: Model-based and data-driven perspectives. *Eng. Struct.*, 199.

Le, T. H. and Caracoglia, L. (2015a). Reduced-order wavelet-Galerkin solution for the coupled, nonlinear stochastic response of slender buildings in transient winds. *J. Sound Vib.*, 344:179–208.

Le, T. H. and Caracoglia, L. (2015b). Wavelet-Galerkin analysis to study the coupled dynamic response of a tall building against transient wind loads. *Eng. Struct.*, 100:763–778.

Le, T. H. and Caracoglia, L. (2017). Computer-based model for the transient dynamics of a tall building during digitally simulated Andrews AFB thunderstorm. *Comput. Struct.*, 193:44–72.

Michaelov, G., Lutes, L. D., and Sarkani, S. (2001). Extreme value of response to nonstationary excitation. *J. Eng. Mech.*, 127(April):352–363.

Roncallo, L. and Solari, G. (2020). An evolutionary power spectral density model of thunderstorm outflows consistent with real-scale time-history records. *J. Wind Eng. Ind. Aerodyn.*, 203(April):104204.

Roncallo, L., Solari, G., Muscolino, G., and Tubino, F. (2022). Maximum dynamic response of linear elastic SDOF systems based on an evolutionary spectral model for thunderstorm outflows. *J. Wind Eng. Ind. Aerodyn.*, 224:104978.

Simiu, E. and Scanlan, R. H. (1996). *Wind effects on structures: Fundamentals and application to design*. Third edit edition.

Solari, G. (1988). Equivalent wind spectrum technique: Theory and applications. *J. Struct. Eng.*, 114(6):1303–1323.

Solari, G. (2016). Thunderstorm response spectrum technique: Theory and applications. *Eng. Struct.*, 108:28–46.

Solari, G., Burlando, M., De Gaetano, P., and Repetto, M. P. (2015a). Characteristics of thunderstorms relevant to the wind loading of structures. *Wind Struct. An Int. J.*, 20(6):763–791.

Solari, G. and De Gaetano, P. (2018). Dynamic response of structures to thunderstorm outflows: Response spectrum technique vs time-domain analysis. *Eng. Struct.*, 176(March):188–207.

Solari, G., De Gaetano, P., and Repetto, M. P. (2015b). Thunderstorm response spectrum: Fundamentals and case study. *J. Wind Eng. Ind. Aerodyn.*, 143:62–77.

Solari, G. and Piccardo, G. (2001). Probabilistic 3-D turbulence modeling for gust buffeting of structures. *Probabilistic Eng. Mech.*, 16(1):73–86.

Vanmarcke, E. H. (1975). on the Distribution of the First-Passage Time for Normal Stationary Random Processes. *Am. Soc. Mech. Eng.*, (75 -APMW-12):215–220.

Vicroy, D. D. (1991). A simple, analytical, axisymmetric microburst model for downdraft estimation. *NASA Tech. Memo. No.104053*.

Vicroy, D. D. (1992). Assessment of microburst models for downdraft estimation. *J. Aircr.*, 29(6):1043–1048.

Wood, G. S., Kwok, K. C. S., Motteram, N. A., and Fletcher, D. F. (2001). Physical and numerical modelling of thunderstorm downbursts. *J. Wind Eng. Ind. Aerodyn.*, 89(2001):535–552.